

**Microphysical features of typhoon and non-typhoon rainfall observed in Taiwan, an island
in the northwest Pacific.**

**Jayalakshmi Janapati¹, Balaji Kumar Seela¹, Pay-Liam Lin^{1,2,3*}, Meng-Tze Lee⁴, Everett
Joseph⁵**

¹Institute of Atmospheric Physics, Department of Atmospheric Sciences, National Central
University, Zhongli district, Taoyuan city, Taiwan

²Earthquake-Disaster & Risk Evaluation and Management Center, National Central University,
Zhongli district, Taoyuan city, Taiwan.

³Research Center for Hazard Mitigation and Prevention, National Central University, Zhongli
district, Taoyuan City, Taiwan

⁴Department of Atmospheric and Oceanic Sciences, McGill University, Montreal, Quebec,
Canada

⁵National Center for Atmospheric Research, Boulder, Colorado

***Correspondence to:**

Prof. Pay-Liam Lin

Institute of Atmospheric Physics, Department of Atmospheric Sciences

National Central University, Zhongli district, Taoyuan City, Taiwan

Phone: 03-422-3294 03-422-7151 ext. 65509

E-mail: tlam@pblap.atm.ncu.edu.tw

Abstract

Information about the raindrop size distribution (RSD) is vital to comprehend the precipitation microphysics, improve the rainfall estimation algorithms, and appraise the rainfall erosivity. Previous research has revealed that the RSD exhibits diversity with geographical location and weather type, which perpetrates to assess the region and weather-specific RSDs. Based on long-term (2004 to 2016) disdrometer measurements in north Taiwan, this study pursued to demonstrate the RSD aspects of summer seasons that were bifurcated into two weather **conditions**, namely typhoon (TY) and non-typhoon (NTY) rainfall. The results show a higher concentration of small drops and a lower concentration of big-size drops in TY compared to NTY rainfall, and this behavior persisted even after characterizing the RSDs into different rainfall rate classes. RSDs expressed in gamma parameters show higher mass-weighted mean diameter (D_m) and lower normalized intercept parameter (N_w) values in NTY than TY rainfall. Forbye, sorting of these two weather **conditions** (TY and NTY rainfall) into stratiform and convective regimes did reveal a large D_m in NTY than the TY rainfall. The RSD empirical relations used in the valuation of rainfall rate ($Z-R$, D_m-R , and N_w-R) and rainfall kinetic energy ($KE-R$, and $KE-D_m$) were enumerated for TY and NTY rainfall, and they exhibited profound diversity between these two weather **conditions**. Attributions of RSD variability between the TY and NTY rainfall to the thermo-dynamical and microphysical processes are elucidated with the aid of reanalysis, remote-sensing, and ground-based datasets.

Keywords: typhoons, non-typhoons, disdrometer, rainfall kinetic energy, north Taiwan

1. Introduction

Taiwan, an island in the northwest Pacific, has complex topography with an outspread from south to north, with an average elevation of about 2 km and peaks of ~ 4 km. The East China Sea bounds Taiwan in the north, the Philippine Sea in the east, Luzon Strait in the south, and the South China Sea in the southwest. This island is affected by two monsoon regimes: southwesterly monsoon (May to August) and northeasterly monsoon (September to April), and these two monsoon regimes were further categorized into winter (December to February), spring (March to April), mei-yu (mid-May to mid-June), summer (mid-June to August), typhoon (May to October), and autumn (September to November) seasons (Chen and Chen, 2003). Among the above-mentioned seasons, the summer seasons, exclusively associated with thunderstorms and typhoons, have intense precipitation than other seasons. Despite reports on the rainfall individualities of different seasons and weather systems in Taiwan (Chen et al., 1999; Chen et al., 2007; Chen et al., 2010; Chen and Chen, 2011; Liang et al., 2017; Tu and Chou, 2013), few attempts were made to explicate rain microphysical aspects, exclusively the RSD characteristics.

The RSDs aid in diverse fields like meteorology, hydrology and remote sensing, and afford an insight into the precipitation microphysics (Rosenfeld and Ulbrich, 2003). Characterization of RSDs offers the opportunity to design radar rainfall estimation algorithms (Ryzhkov and Zrnić, 1995), improve the cloud modeling parameterization (McFarquhar et al., 2015), assess the rainfall erosivity relations (Janapati et al., 2019), validate the remote sensing instruments (Liao et al., 2014; Nakamura and Iguchi, 2007), and appraise the rain attenuations (Chen et al., 2011). Owing to the aforementioned implications of RSDs, ample literature exists on RSDs for spatial, seasonal (Thompson et al., 2015; Jayalakshmi and Reddy, 2014; Seela et al.,

2017;Seela et al., 2018;Krishna et al., 2016;Seela et al., 2016) variations, storm to storm, within the storm (Kumari et al., 2014;Maki et al., 2001;Jung et al., 2012;Bao et al., 2020;Janapati et al., 2017), and different precipitations (Tokay and Short, 1996;Krishna et al., 2016).

Investigations on RSDs have been escalating to illuminate the hydrological (Lin and Chen, 2012;Lu et al., 2008;Janapati et al., 2019;Chang et al., 2017) and microphysical characteristics (Chu and Su, 2008;Jung et al., 2012;Seela et al., 2017;Seela et al., 2018;Lee et al., 2019;Janapati et al., 2020) of diverse precipitating clouds in Taiwan. For instance, Chu and Su (2008) reconnoitered the slope-shape relations for seven precipitation events related to four different weather systems in north Taiwan, and they showed that the derived μ - Λ relation was independent of the gamma RSD moment order. Measurements of a squall line in south Taiwan with ground-based radar and disdrometer revealed that the D_m values in the squall line's convective precipitation were higher than the maritime clusters (Jung et al., 2012). Chang et al. (2009) analyzed the RSDs of landfall typhoons in north Taiwan, and they opined that the interaction of typhoons with Taiwan's complex terrain resulted in the RSDs intermediate to maritime and continental clusters. The comparison study of summer seasons' RSDs between Taiwan and Palau Islands by Seela et al. (2017) revealed more large drops in Taiwan than Palau, and they contended that deeply extended convective clouds with more aerosols in Taiwan resulted in the differences between these two Islands. With the aid of long-term disdrometer measurements for summer and winter seasons in north Taiwan, Seela et al. (2018) noticed a profound disparities in RSDs between these two seasons, and they established the attribution of RSDs differences to the microphysical processes concomitant with deep convective clouds in summer and warm clouds in winter. Furthermore, investigations on microphysical features of six seasons (winter, spring, mei-yu, summer, typhoon, and autumn) in north Taiwan divulged the

highest mean D_m values in the summer and highest concentration ($\log_{10}N_w$) in the winter (Lee et al., 2019). A recent study on Indian and Pacific Ocean tropical cyclones manifested higher D_m values in Pacific Ocean tropical cyclones than the Indian Ocean tropical cyclones (Janapati et al., 2020).

Efforts have been performed to reveal the RSDs characteristics of tropical cyclones and non-tropical cyclones in India, Australia, China, and Japan (Radhakrishna and Narayana Rao, 2010; Kumar and Reddy, 2013; Deo and Walsh, 2016; Chen et al., 2019; Chen et al., 2017). Analysis of tropical cyclones and non-tropical cyclones RSDs in Gadanki (Radhakrishna and Narayana Rao, 2010) and Kadapa (Kumar and Reddy, 2013) unveiled a higher concentration of small drops in tropical cyclones than the non-tropical cyclones. In Australia, Deo and Walsh (2016) illustrated the tropical cyclones and non-tropical cyclones RSDs and demonstrated higher D_m values in non-tropical cyclones than tropical cyclones rainfall. From the 2DVD measurements in East china, Chen et al. (2017) appraised the polarimetric radar variables for typhoons, Mei-yu, and squall line precipitations, and they revealed discrete alterations among these weather systems. Over south China, distinct differences in rain integral parameters of typhoons and squall lines were perceived by Zhang et al. (2019), and they concluded that it is essential to adopt precipitation specific rainfall estimators. Examination of typhoons and mei-yu season RSDs in Japan affirmed maritime behavior in typhoons and continental behavior in mei-yu rainfall (Chen et al., 2019).

In contempt of investigations on the typhoon and non-typhoon **weather conditions'** rainfall characteristics (Chen and Chen, 2011; Tu and Chou, 2013), the microphysical features, especially the summer seasons' RSDs (explicitly segregated to typhoon and non-typhoon

weather conditions) are yet to be documented for the Taiwan region. On this account, this study sought to address the following objectives: 1. To investigate alike or unlike individualities of RSDs between the typhoon and non-typhoon rainfall, 2. To identify comparable/unrelated features of typhoon and non-typhoon rainfall to the previous studies, 3. quantification of rainfall rate and rainfall kinetic energy relations, 4. To discern conceivable rationale for peculiarities in the RSDs between typhoon and non-typhoon rainfall events. In this context, to address the aforementioned objectives for the typhoons and non-typhoons rainfall, long-term disdrometer, radar, remote-sensing, and re-analysis data sets were used.

2. Data sets used

Taiwan geographic map with National Central University (NCU) (24° 58' N, 121° 10' E) site (indicated with a filled green circle), where the Joss–Waldvogel disdrometer (JWD) (Joss and Waldvogel, 1969) measurements were conducted [for the summer season (16 June to -31 August) rainy days of the years 2004 to 2016], is shown in Fig.1. The disdrometer measurements in summer seasons were further classified into a typhoon (TY) and non-typhoon (NTY) regimes. In identifying the rainfall amounts of typhoons over Taiwan, previous studies adopted different criteria (Tu and Chou, 2013; Chu et al., 2007; Chen et al., 2010). For instance, if a typhoon center was invaded the rectangular grid box of 21°-26° N and 119°-125° E (Chu et al., 2007) or 19.5°-27.5° and 117.5°-124.5° E (Chen et al., 2010) or 18°-29.5° N and 116°-126° E (Tu and Chou, 2013), the corresponding rain in Taiwan was selected as typhoon induced rain. On the other hand, in the current study, precipitation at the NCU disdrometer site was considered as typhoon-induced rain when the typhoon center was ≤ 500 km from the disdrometer (Janapati et al., 2019),

and the rest of the rainy days in summer seasons were categorized as NTY rainy days. With this condition, a total number of 59 TY rainy days (hereafter TY days) and 131 NTY rainy days (hereafter NTY days) were recorded by the NCU JWD from 2004 to 2016 (excluding 2008 and 2009 years).

The JWD has its advantage and disadvantages over the other disdrometers (Lee and Zawadzki, 2005; McFarquhar and List, 1993; Sauvageot and Lacaux, 1995; Sheppard, 1990; Sheppard and Joe, 1994; Tokay et al., 2001; Tokay et al., 2013). For instance, JWD can't measure fall velocity; hence, to evaluate the RSD parameters from the JWD, we assumed that raindrops reach the ground with terminal velocity. Further, in heavy rainfall events, the JWD measures the spurious values for the raindrops of diameter < 1 mm, and it was named as the dead-time of the instrument. To deal with the dead-time of the JWD, the manufacturer provided an error correction multiplication matrix based on a correction scheme from Sheppard and Joe (1994). However, as the JWD can't record any drops for the first three to four channels in heavy rainfall events, the multiplicative matrix algorithm does not increase the counts when the channel has no drops (Tokay & Short, 1996; Tokay et al., 2001); hence, in this study, we didn't apply the dead-time correction to the JWD data. On top of that, 1-min RSD samples with raindrops count < 10 and rainfall rate $< 0.1 \text{ mm h}^{-1}$ were discarded (Tokay & Short, 1996). The daily rainfall accumulations from the JWD are related to the collocated rain gauge for both TY and NTY rain regimes and are illustrated with scatter plots in Fig.2. The rainy days (TY: 04 days and NTY: 0 days) with larger discrepancy between JWD and rain gauge measurements were discarded in this study. Further, we compared the JWD measurements (for both TY and NTY rainy days) with the rain gauge for different wind speed conditions (daily maximum wind speed: 0-8, 8-14, 14-18, $> 18 \text{ m s}^{-1}$), and the results are provided in Table 1. For the considered NTY rainy days, the daily

maximum wind speeds were less than 14 m s^{-1} , however, there were TY rainy days with wind speed $> 18 \text{ m/s}$. A good agreement between JWD and rain gauge measurements for both TY and NTY days (Fig.2 and Table 1) provided the trustworthiness of the JWD data for further analysis.

The rain/RSD parameters like raindrop concentration $N(D)$ ($\text{mm}^{-1} \text{ m}^{-3}$), radar reflectivity factor Z ($\text{mm}^6 \text{ m}^{-3}$), liquid water content W (g m^{-3}), rainfall rate R (mm h^{-1}), total number concentration N_t (m^{-3}), normalized intercept parameter, N_w ($\text{m}^{-3} \text{ mm}^{-1}$), shape parameter μ (-), slope parameter λ (mm^{-1}), and mass-weighted mean diameter D_m (mm) are estimated from the JWD measurements. The formulations for these rain/RSD parameters are detailed in Seela et al. (2017);Seela et al. (2018);Tokay et al. (2001);Bringi et al. (2003);Tokay and Short (1996). In addition to rain parameters, the rainfall kinetic energy (KE), which can be expressed in KE flux (KE_{time} , in $\text{J m}^{-2} \text{ h}^{-1}$) and KE content (KE_{mm} , $\text{J m}^{-2} \text{ mm}^{-1}$) were computed for TY and NTY rainfall using the procedures of Fornis et al. (2005);Salles et al. (2002);van Dijk et al. (2002).

In addition to disdrometer data, remote-sensing (TRMM and MODIS) and reanalysis (ERA-interim) data sets are used to elucidate the thermodynamical and microphysical characteristics that are accountable for the possible disparities in RSDs between TY and NTY rainfall. Bright band and storm heights from TRMM satellite (2A23 data product) (Iguchi et al., 2000;Kummerow et al., 2001), cloud effective radii (CER) of liquid and ice particles from MODIS satellite (MOD08_D3 data product) (Platnick et al., 2015;Remer et al., 2005;Nakajima and King, 1989), water vapor, convective available potential energy (CAPE), relative humidity and temperature profiles from ERA-Interim (Dee et al., 2011) are considered for TY and NTY rainfall. Both remote-sensing and reanalysis data sets are interpolated to $0.125^\circ \times 0.125^\circ$ over the

disdrometer site. A brief description of these data sets can be found in Seela et al. (2018);Janapati et al. (2020).

Besides remote-sensing and re-analysis data sets, the radar reflectivity profiles from radars mosaic are used to reveal TY and NTY rainfall characteristics. The Z profiles were obtained from the six ground-based radars, and the locations of these radars are depicted with red triangles in Fig. 1. Over the JWD site, the reflectivity profiles available for the period of 2005-2014 are used, and further details on Taiwan radar reflectivity mosaic can be found in Chang et al. (2020).

3. Observational Results

The quality controlled JWD data showed 23074 and 20368 minutes of RSD samples, respectively, for TY and NTY rainfall, and the mean raindrops concentrations of these two weather conditions are depicted in Fig. 2. In this work, raindrops of diameter greater than 3 mm, 1–3 mm, and less than 1 mm are named, respectively, as large, mid, and small drops (Tokay et al., 2008;Seela et al., 2018). As illustrated in Fig. 3a, perceivable segregation between TY and NTY rainfall RSDs can be seen with more large drops in NTY than the TY rainfall. Despite of weak distinction between TY and NTY mean rain spectra for raindrops of diameter < 2 mm, it can be seen that the spectra variability within TY and NTY classes is smaller than the differences between averaged TY and NTY spectra. Given the dependency of raindrop concentration on rainfall rate, it is difficult to interpret alterations between TY and NTY rainfall RSD from Fig. 3a. Consequently, we implemented the normalization procedure (Testud et al., 2001), which is

independent of the shape of the observed raindrop spectra, to the TY and NTY RSDs. For TY and NTY rainfall, the drop diameter (D , mm) and raindrop concentrations [$N(D)$, $\text{mm}^{-1} \text{m}^{-3}$] are normalized, respectively, by mass-weighted mean diameter (D_m , mm) and normalized intercept parameter (N_w , $\text{mm}^{-1} \text{m}^{-3}$), and these normalized RSDs are illustrated in Fig. 3b. A remarkable departure in the normalized RSDs spectra between NTY and TY rainfall (for $D/D_m > 2$) insinuates that divergent microphysical processes were involved in these two weather conditions.

For TY and NTY rainfall, the probability density functions (PDFs) are evaluated for D_m (mass-weighted mean diameter in mm), $\log_{10}N_w$ (N_w is normalized intercept parameter in $\text{mm}^{-1} \text{m}^{-3}$), $\log_{10}R$ (R is rainfall rate in mm h^{-1}), and $\log_{10}W$ (W is the liquid water content in g m^{-3}) and are depicted in Fig. 4. Fig. 4a demonstrates the PDF of D_m in NTY rainfall has higher distribution than TY rainfall for $D_m > 1.7$ mm. The $\log_{10}N_w$ ($\log_{10}R$) PDF distribution shows peak values around 3.7 (0.3) and 3.4 (0), respectively, for TY and NTY rainfall (Fig. 4b). The PDF of $\log_{10}W$ shows a higher percentage at lower $\log_{10}W$ values ($\log_{10}W < -1$) in NTY rainfall, and a higher percentage at higher $\log_{10}W$ values ($\log_{10}W > -1$) in TY rainfall (Fig. 4d). Further, a statistical Student's t-test (used to determine whether two data sets are significantly different from each other or not), is executed between TY and NTY rainfall D_m values. The test results rejected the null hypothesis at 0.05 and 0.01 significance levels, which confirm that the D_m values in TY rainfall are different from that of the NTY rainfall. Similarly, the Student's t-test performed for other three parameters ($\log_{10}N_w$, $\log_{10}R$, and $\log_{10}W$) also showed that these parameters in TY rainfall are different from that of the NTY rainfall.

3.1 Contribution of raindrop diameters to N_t and R

The contributions of raindrop diameter classes (diameter < 1 mm, 1–2 mm, 2–3 mm, 3–4 mm, and 4–5 mm) to N_t (m^{-3}) and R (mm h^{-1}) for TY and NTY rainfall are shown in Fig. 5. As can be seen in Fig.5a & b, for both TY and NTY rainfall, with the increase of drop diameter classes, contribution to total number concentration decreases, while that of rainfall rate increases and then lessens, and such peculiarities were noticed by previous researchers on tropical cyclones (Chen et al., 2019) and summer season rainfall (Wu et al., 2019). For both TY and NTY rainfall, small size drops (< 1 mm) grant to large number concentration (> 70%) and about 10% to rainfall rate. For both TY and NTY rainfall, raindrops with diameter 1–2 mm afford around 20% to number concentration; nonetheless, these raindrops (1–2 mm) yield around 60% (55%) to rainfall rate for TY (NTY) rainfall. The contribution of raindrops with diameters 2–3 mm to number concentration is negligible, and the rainfall rate is above 20% for both TY and NTY rainfall. Fig. 5a&b emphasize the predominant contribution of small (< 1 mm) and mid-size drops (1–3 mm) to total number concentration and rainfall rate than large drops. The occurrence percentages of N_t (m^{-3}) ($[(N_t)_{\text{TY}} \text{ or } (N_t)_{\text{NTY}} / ((N_t)_{\text{TY}} + (N_t)_{\text{NTY}})] \times 100$) and R (mm h^{-1}) ($[(R)_{\text{TY}} \text{ or } (R)_{\text{NTY}} / ((R)_{\text{TY}} + (R)_{\text{NTY}})] \times 100$) at different diameter classes are illustrated, respectively, in Fig.5c and Fig.5d. For the first three drop diameter classes (< 1 mm, 1–2 mm, 2–3 mm), the N_t (m^{-3}) percentages are predominant in TY than NTY rainfall, and in contrast, for large drops (> 3 mm), the N_t (m^{-3}) percentages are higher in NTY than TY rainfall. Similar to the N_t (m^{-3}), the rainfall rate percentages are higher in TY than NTY rainfall for small and mid-size drops, and an opposite feature can be seen for large drops (> 3 mm).

3.2 Segregation of RSDs based on rainfall rates

To further explore the discrepancies between TY and NTY rainfall RSDs, we segregate the TY and NTY RSDs into seven rainfall rate classes (as given in Table 2) using the below-mentioned grouping criteria. The data points in each rainfall rate category should be sufficiently large in TY and NTY rainfall, and for each category, the mean values of rainfall rates should be nearly equal between these two weather conditions (TY and NTY rainfall) (Jayalakshmi and Reddy, 2014;Deo and Walsh, 2016;Seela et al., 2017). Statistical values of these seven rainfall rate categories are specified in Table 2 for TY and NTY rainfall. As depicted in the table, the mean values of rainfall rates are nearly equal between these two weather conditions (TY and NTY). Excluding fourth and fifth rainfall rate class (C4 and C5), the skewness values are excessive in NTY than TY rainfall. Correspondingly, these two weather conditions (TY and NTY) show positive skewness designating that the rainfall rates are focused on the left to the mean. The RSDs peculiarities between TY and NTY rainfall are evaluated in percentage parameter (Ratio of $N(D)$ in TY or NTY rainfall for the raindrop diameter D and rainfall rate class R to the raindrop concentration accumulations in TY and NTY rainfall) context, as explicated in Seela et al. (2018). The percentage parameter of $N(D)$ for different rain rate class, $\delta(D, R)=\delta(D, R_{ck})_{TY/NTY}$ is given as

$$\delta(D, R_{ck})_{TY} = \frac{[N(D)_{TY}]_{ck}}{([N(D)_{TY}]_{ck}+[N(D)_{NTY}]_{ck})} \times 100 \quad \text{-----(1)}$$

$$\delta(D, R_{ck})_{NTY} = \frac{[N(D)_{NTY}]_{ck}}{([N(D)_{TY}]_{ck}+[N(D)_{NTY}]_{ck})} \times 100 \quad \text{-----(2)}$$

Where $[N(D)_{TY}]_{ck}$ or $[N(D)_{NTY}]_{ck}$ represents the mean $N(D)$ of TY or NTY rainfall for the rain rate class “Ck”, with k=1, 2, 3, 4, 5, 6, 7 (C1: $0.1 \leq R < 1$, C2: $1 \leq R < 2$, C3: $2 \leq R < 5$, C4: $5 \leq$

264 $R < 10$, C5: $10 \leq R < 30$, C6: $30 \leq R < 50$, and C7: $R > 50$, where R is in mm h^{-1} ; please refer to
265 table 2).

266 The raindrop concentration percentages are appraised for both TY and NTY rainfall and are
267 illustrated in Fig. 6. The percentage contribution of $N(D)$ for TY and NTY rainfall corroborated
268 that small and mid-size drops (< 3 mm) display superior percentage in TY than NTY rainfall.
269 Nevertheless, large drops (> 3 mm) unveil a higher percentage of $N(D)$ in NTY than TY rainfall.

270 Distributions of D_m (mm) and $\log_{10}N_w$ ($\text{m}^{-3} \text{mm}^{-1}$) for seven rainfall rate classes are
271 depicted with box plots in Fig. 7. As can be seen from Fig. 7a, with the increase in rainfall rate
272 class, D_m values increase for both TY and NTY rainfall, which is due to a raise in large size
273 drops concentration and a reduction in small drops concentration (Rosenfeld and Ulbrich,
274 2003; Krishna et al., 2016), and similar finding were noticed by previous researchers for both
275 tropical cyclones and non-tropical cyclones rainfall (Bao et al., 2020; Deo and Walsh,
276 2016; Jayalakshmi and Reddy, 2014; Radhakrishna and Narayana Rao, 2010). On the other hand,
277 D_m values are greater in NTY than TY rainfall in all rainfall rate classes due to the predominant
278 concentration of mid-size and small size raindrops in TY than NTY days (Fig.6). Compared to
279 D_m , for all seven rainfall rate classes, the $\log_{10}N_w$ values are higher in TY than NTY rainfall
280 (Fig.7b).

281 Scatter plots for D_o [$D_o = (3.67 + \mu)/A$] and $\log_{10}N_w$ values in different rainfall rate classes
282 (< 5 , $5-10$, $10-30$, $30-50$, and > 50 mm h^{-1}) are depicted in Fig.8a and Fig.8b, respectively, for
283 TY and NTY rainfall. Likewise, the mean values of D_o and $\log_{10}N_w$ in different rainfall rate
284 classes for TY and NTY rainfall are depicted, respectively, in Fig. 8c and Fig.8d. The stratiform
285 and convective classification lines of Thompson et al. (2015) and Bringi et al. (2009) are

designated, respectively, with horizontal black dotted line and slant solid line in Fig.8. With the enhancement in the rainfall rate class, D_o and $\log_{10}N_w$ distributions are narrowed for both TY and NTY rainfall. For rainfall rates $> 10 \text{ mm h}^{-1}$ and $< 10 \text{ mm h}^{-1}$, the D_o and $\log_{10}N_w$ data points are distributed, respectively, in the convective and stratiform region of Bringi et al. (2009) (Fig. 8a &b). With the rise in the rainfall rate class, the mean D_o values increase for both TY and NTY rainfall. Besides, for $R > 10 \text{ mm h}^{-1}$, mean D_o and $\log_{10}N_w$ values are scattered in the convective region of Bringi et al. (2009) (Fig. 8c & d). As depicted in Fig. 8c &d, for rainfall rates $> 10 \text{ mm h}^{-1}$, TY (NTY) rainfall mean $\log_{10}N_w$ values are scattered over (below) the rainfall classification line of Thompson et al. (2015) (Fig. 8c & d), and this exhibits that to segregate the TY and NTY rainfall to stratiform and convective type, Bringi et al. (2009) classification method is superior to Thompson et al. (2015).

3.3 RSDs in precipitation types

Ample literature showed distinctiveness in the RSDs with precipitation type, and numerous methods were documented to segregate the precipitation into stratiform and convective type (Ma et al., 2019; Jayalakshmi and Reddy, 2014; Ulbrich and Atlas, 2007). For instance, Tokay and Short (1996) reported variations in convective precipitations to that of the stratiform regimes. Some studies emphasized the importance to adopt precipitation specific rainfall estimation relations (Ulbrich and Atlas, 2007). In separating the TY and NTY rainfall into stratiform and convective type, we adopted the modified form of Bringi et al. (2003) classification method as mentioned in Ma et al. (2019). Distributions of mean $N(D)$ ($\text{m}^{-3} \text{mm}^{-1}$) with raindrop diameters for TY and NTY rainfall are depicted in Fig. 9a. Except for the first drop

size bin, higher drop concentrations are noticed for convective rainfall than the stratiform rainfall. Concave shaped $N(D)$ with broader distribution in convective than stratiform is due to the breakup of large drops by collisions (Hu and Srivastava, 1995). The RSD characteristics demonstrated by the stratiform and convective precipitations show similar features to that of the earlier studies for continental (Jayalakshmi and Reddy, 2014) and oceanic regions (Krishna et al., 2016). On the other hand, in stratiform and convective regimes, the mid-size and large drops concentration is higher in NTY than TY rainfall. Variations in D_m and $\log_{10}N_w$ for both precipitations of TY and NTY are depicted in Fig. 9b. The maritime and continental convective clusters of Bringi et al. (2003) are depicted with gray rectangles. For both TY and NTY rainfall, larger mean D_m and $\log_{10}N_w$ values are noticed for convective precipitation. In contrast to that, in stratiform and convective regimes, the NTY rainfall exhibit smaller $\log_{10}N_w$ and larger D_m values than TY rainfall.

3.4 Rainfall estimation relations

Uncertainties in the estimation of rainfall from weather radars can be minimized through region, weather system, and precipitation specific radar reflectivity and rainfall rate ($Z-R$) relations. In $Z = A R^b$ relation, size of the raindrops can be inferred from the coefficient 'A', and the exponent 'b' represents microphysical process (Atlas et al., 1999; Steiner et al., 2004; Atlas and Williams, 2003). The TY and NTY rainfall $Z-R$ relations are derived from the linear regression applied to $10 \cdot \log_{10} R$, and Z , and are provided in Fig. 10. The coefficient values of $Z-R$ relations are larger in NTY than the TY for stratiform and convective precipitations, as well as for total rainfall. This variation is due to the presence of significant number of large size drops

in NTY to that of the TY rainfall. The current TY rainfall $Z-R$ relations show disparity with the other locations tropical cyclones rainfall relations (Bao et al., 2020; Wen et al., 2018; Janapati et al., 2020). The possible reasons for the variations in other locations' tropical cyclones $Z-R$ relations to that of the present TY rainfall could be due to geographical variations or the RSD measurements from different types of disdrometers (Adirosi et al., 2018). Moreover, the obtained TY and NTY days $Z-R$ relations are found to differ from the default ($Z=300 R^{1.4}$) and tropical $Z-R$ relationships ($Z=250R^{1.2}$), which suggests to adopt weather and region-specific $Z-R$ relations.

3.5 The rainfall rate relationships with D_m and N_w

The normalized intercept parameter and mass-weighted mean diameter values can provide the RSD features, and these parameters were found to show uniqueness with the rainfall rate (Chen et al., 2016; Janapati et al., 2020). Distribution of D_m and $\log_{10}N_w$ with rainfall rates for both weather conditions are portrayed in Fig. 11. As can be seen from the figure, the distributions of D_m gets narrowed with the increase in rainfall rates for both weather conditions, and such behaviors were reported for tropical cyclone and summer season rainfall (Kumar and Reddy, 2013; Wen et al., 2018; Chang et al., 2009; Janapati et al., 2020; Chen et al., 2019; Wu et al., 2019). No further fluctuations in the D_m values at higher rainfall rates ($> 25 \text{ mm h}^{-1}$) are due to the equilibrium condition in the RSDs (attained through raindrop breakup and coalescence processes) (Hu and Srivastava, 1995), and further increase in rainfall rates is due to the increase in number concentration under RSDs equilibrium condition (Bringi and Chandrasekar, 2001). The power-law equations for D_m-R and $\log_{10}N_w-R$ are computed using a non-linear least squares

method and are exemplified in Fig. 11. The evaluated D_m – R ($\log_{10}N_w$ – R) relations exhibit a larger (smaller) coefficient in NTY rainfall than TY rainfall, which confirm that for given rainfall rates, the NTY rainfall had a higher D_m and lower N_w values than the TY rainfall.

3.6 KE – R and KE – D_m relations

The raindrops reaching the ground with a certain amount of kinetic energy (KE) can erode the soil from the ground surface. Hence, the raindrops KE or rainfall KE is one of the critical physical quantities in soil erosion studies (Wischmeier, 1959; Kinnell, 1981). As the rainfall KE is related to the raindrop diameter and its fall velocity, it can be evaluated through the RSD information (Kinnell, 1981). The empirical relations between the rainfall KE and rainfall intensity are incorporated in assessing the rainfall erosivity factor (R-factor), one of the key parameters in soil erosion modeling studies (Renard et al., 1997; Janapati et al., 2019). To this end, we investigated the empirical relations between the rainfall KE (KE_{time} in $J\ m^{-2}\ h^{-1}$; KE_{mm} in $J\ m^{-2}\ mm^{-1}$) and rainfall rate ($mm\ h^{-1}$) using non-linear least-squares regression method for TY and NTY rainfall. The distribution plots of KE_{mm} and KE_{time} with R for TY and NTY rainfall are portrayed in Fig. 12. The KE_{time} – R empirical relations are derived by fitting the data points with power and liner methods. For both TY and NTY days, the power-law line fitted well by passing through the middle of the data points at both lower and higher rainfall rates than the linear fit line (Fig. 12a & b). The KE_{mm} and R data points are fitted with power, logarithmic, and exponential law. Among three forms of relations, the power-law fitted well with the data points for both TY and NTY days (Fig. 12c & d). Moreover, empirical relations between D_m (mm), the KE_{mm} are evaluated for both TY and NTY rainfall and are given in Fig. 13. Comparison of present KE – D_m

relations with the East China seasonal rainfall $KE-D_m$ ($KE = -2.33D_m^2 + 21.05D_m - 7.79$) relation shows that both TY and NTY relations in Taiwan are different from that of East China (Wen et al., 2019). The derived $KE-D_m$ relations can be used to estimate the KE values from the remote-sensing radar (GPM DPR) measurements. The $KE_{time}-R$, $KE_{mm}-R$, and $KE-D_m$ relations and their statistical values are given in Table 3. For both $KE_{time}-R$, $KE_{mm}-R$ relations, the power-law exhibits higher CC and lower RMSE and NRMSE values, which suggest to adopt the power form equation to estimate the rainfall KE .

4. Discussion

To apprehend propitious mechanisms responsible for the discrepancies in RSDs between TY and NTY rainfall, re-analysis, remote sensing, and ground-based radar data sets are used. The water vapor and CAPE values for TY and NTY days depicted with a box plot in Fig. 14 signify that NTY days had strong convective activity with vigorous updrafts and downdrafts than TY days. Nonetheless, if we look at the storm and bright band heights (BBH) (Fig. 15), TY days had relatively higher BBH than NTY days and there is no apparent alterations in storm heights between TY and NTY days. Relatively higher BBH support the greater CER values for ice particles in TY than NTY days (Fig. 16b). Nevertheless, there is no much difference in the liquid particles CER median values between TY and NTY days (Fig. 16a). The deep stratiform clouds in TY days offer sufficient time for the growth of ice crystals to large size (via aggregation and vapor deposition) and melt to big size drops once they cross the melting layer. Relatively higher BBH in TY days allowed the RSDs to reach equilibrium through various microphysical processes (collision, coalescence, and breakup) than NTY rainfall (Hu and Srivastava, 1995). In

contrast, intense convection (with resilient updrafts and downdrafts) in NTY days enhances raindrops growth (through collision-coalescence and drop sorting processes), shoots smaller drops at higher altitudes, and allows large drops to reach the surface. The vertical profiles of air temperature and relative humidity for TY and NTY days evidently illustrate that NTY days were drier compared to that of the TY rainy days (Fig. 17), and hence, the rate of evaporation of small drops (that were produced through the collision breakup processes) in NTY days was higher than TY days resulting in more large drops in NTY days.

The radar reflectivity CFAD (contoured frequency-by-altitude diagrams) for (a) typhoon (TY) and (b) non-typhoon (NTY) days are portrayed in Fig. 18. The vertical sky blue (dark magenta) star line in Fig. 18a (Fig.18b) is the mean radar reflectivity profile of TY (NTY) days. The white-star dotted profile in Fig.18a & b is the mean of both TY and NTY days' reflectivity profiles. The mean reflectivity profile of TY (NTY) days is less (higher) than the mean of TY and NTY days' reflectivity profile. A higher occurrence percentage of lower Z values ($Z < 10$ dBZ) in TY than NTY days can be seen at higher altitudes. In contrast to that, below the melting layer, the occurrence percentage of higher reflectivity values ($Z > 40$ dBZ) is higher in NTY than TY days. The mean vertical profiles of radar reflectivity for TY and NTY days are plotted in Fig. 19. It can be seen from the figure that the mean reflectivity values are higher in NTY than TY days. As the radar reflectivity is directly related to the sixth power of raindrop diameter, higher reflectivity profiles in NTY than TY days infer the predominance of large drops in NTY than TY rainy days. The above-mentioned microphysical and thermodynamical processes resulted in more big size drops and few small drops in NTY than TY days, resulting in higher D_m and lower N_w values in NTY than TY days.

5. Summary and conclusions

Raindrop size distributions (RSDs) of typhoon (TY) and non-typhoon (NTY) rainy days have been analyzed using long-term (2004-2016) disdrometer measurements from north Taiwan. Besides disdrometer data, other auxiliary data sets (remote-sensing, re-analysis, and ground-based radar) have been used to discuss the disparities in RSDs between TY and NTY rainfall. The NTY days have more big size drops and less small size drops than TY days, resulting in larger D_m and smaller N_w values in NTY days. The mean normalized RSD of NTY precipitation has a higher occurrence of larger drops (at $D/D_m > 2$) than TY precipitation, which indicates the possibility for diverse microphysical processes between these two weather conditions. The classification of RSDs to varying rainfall rates and precipitation (stratiform and convective) regimes clearly show smaller D_m and larger N_w values in TY than NTY days. The percentage contribution of large (small and mid-size) drops to N_t and R is lower (higher) in TY than NTY rainfall. For both TY and NTY rainy days, stratiform precipitations D_m and N_w values are smaller than the maritime and continental clusters, while, convective precipitations D_m values are approximately within the range of maritime clusters. The rainfall kinetic energy and intensity ($KE_{time}-R$ and $KE_{mm}-R$) relations evaluated for both TY and NTY rainy days reveal greater performance of power relation than other types, and confirms to use power form of $KE-R$ relations in assessing the rainfall erosivity factor for TY and NTY rainfall events. The enumerated $Z-R$, D_m-R , N_w-R , $KE_{time}-R$, $KE_{mm}-R$, and $KE_{mm}-D_m$ relations showed profound diversity between TY and NTY rainfall and substantiate the significance of adopting precipitation specific empirical relations in evaluating the rainfall rate and kinetic energy values. Overall, present study confirms that relatively higher convective activity with drier conditions in NTY than TY days significantly wedged the disparities in RSDs with dissimilar microphysical

processes. The current observational outcomes could benefit in appraising the radar precipitation estimation algorithms, cloud modeling, and rainfall erosivity in north Taiwan for TY and NTY rainfall events.

Data availability. The Era-interim re-analysis data can be obtained from <https://www.ecmwf.int/en/forecasts/datasets/reanalysis-datasets/era-interim>. The TRMM data can be retrieved from <https://gpm.nasa.gov/data/directory>. The MODIS cloud data product can be accessed through <https://modis.gsfc.nasa.gov/data/dataproduct/mod06.php>. The ground-based radar and disdrometer data are available from the corresponding author upon reasonable request.

Author contributions. JJ and BKS conceptualized the idea; PLL and EJ provided funding acquisition, project administration, and observation data; JJ, BKS, and MTL conducted the detailed analysis; PLL, and EJ supervised the analysis; JJ, BKS wrote the initial manuscript; JJ, BKS, PLL reviewed and revised the manuscript; all authors involved in writing the manuscript and revisions.

Competing interests. No conflict of interest is declared by the all authors.

460 *Acknowledgements.* We acknowledge the Central Weather Bureau (CWB) of Taiwan, in
461 facilitating the radar reflectivity data, and Tropical Rainfall Measuring Mission (TRMM), ERA-
462 Interim and MODIS research team for their efforts in providing the data. This research work is
463 carried out under the Taiwan Ministry of Science and Technology (MOST) grant numbers:
464 MOST 108-2111-M-008-028, MOST 108-2625-M-008-011, MOST: 104-2923-M-008-003 and
465 partially by “Earthquake-Disaster & Risk Evaluation and Management Center, E-DREaM” from
466 The Featured Areas Research Center Program within the framework of the Higher Education
467 Sprout Project by the Ministry of Education (MOE), Taiwan. The first author, JJ is supported by
468 the grant number MOST 108–2811–M–008–558, and second author, BKS, by MOST 108-2625-
469 M-008-011 and MOST 108-2811-M-008-595.

References

- Adirosi, E., Roberto, N., Montopoli, M., Gorgucci, E., and Baldini, L.: Influence of Disdrometer Type on Weather Radar Algorithms from Measured DSD: Application to Italian Climatology, *Atmosphere-Basel*, 9, 360, 10.3390/atmos9090360, 2018.
- Atlas, D., Ulbrich, C. W., Marks Jr, F. D., Amitai, E., and Williams, C. R.: Systematic variation of drop size and radar-rainfall relations, *Journal of Geophysical Research: Atmospheres*, 104, 6155-6169, 10.1029/1998JD200098, 1999.
- Atlas, D., and Williams, C. R.: The Anatomy of a Continental Tropical Convective Storm, *Journal of the Atmospheric Sciences*, 60, 3-15, 10.1175/1520-0469(2003)060<0003:Taoact>2.0.Co;2, 2003.
- Bao, X., Wu, L., Zhang, S., Li, Q., Lin, L., Zhao, B., Wu, D., Xia, W., and Xu, B.: Distinct Raindrop Size Distributions of Convective Inner- and Outer-Rainband Rain in Typhoon Maria (2018), *Journal of Geophysical Research: Atmospheres*, 125, e2020JD032482, 10.1029/2020jd032482, 2020.
- Bringi, V., Williams, C., Thurai, M., and May, P.: Using dual-polarized radar and dual-frequency profiler for DSD characterization: A case study from Darwin, Australia, *Journal of Atmospheric and Oceanic Technology*, 26, 2107-2122, 2009.
- Bringi, V. N., and Chandrasekar, V.: *Polarimetric Doppler Weather Radar: Principles and Applications*, Cambridge University Press., 2001.

490 Bringi, V. N., Chandrasekar, V., Hubbert, J., Gorgucci, E., Randeu, W. L., and Schoenhuber, M.:
491 Raindrop Size Distribution in Different Climatic Regimes from Disdrometer and Dual-
492 Polarized Radar Analysis, *Journal of the Atmospheric Sciences*, 60, 354-365,
493 10.1175/1520-0469(2003)060<0354:RSDIDC>2.0.CO;2, 2003.

494 Chang, J. M., Chen, H. E., Jou, B. J. D., Tsou, N. C., and Lin, G. W.: Characteristics of Rainfall
495 Intensity, Duration, and Kinetic Energy for Landslide Triggering in Taiwan, *Engineering*
496 *Geology*, 231, 81-87, 10.1016/j.enggeo.2017.10.006, 2017.

497 Chang, P.-L., Zhang, J., Tang, Y.-S., Tang, L., Lin, P.-F., Langston, C., Kaney, B., Chen, C.-R.,
498 and Howard, K.: An Operational Multi-Radar Multi-Sensor QPE System in Taiwan,
499 *Bulletin of the American Meteorological Society*, 1-56, 10.1175/bams-d-20-0043.1, 2020.

500 Chang, W.-Y., Wang, T.-C. C., and Lin, P.-L.: Characteristics of the Raindrop Size Distribution
501 and Drop Shape Relation in Typhoon Systems in the Western Pacific from the 2D Video
502 Disdrometer and NCU C-Band Polarimetric Radar, *Journal of Atmospheric and Oceanic*
503 *Technology*, 26, 1973-1993, 10.1175/2009jtecha1236.1, 2009.

504 Chen, B., Wang, J., and Gong, D.: Raindrop size distribution in a midlatitude continental squall
505 line measured by thies optical disdrometers over East China, *J. Appl. Meteor. Climatol.*,
506 55, 621–634, 10.1175/JAMC-D-15-0127.1, 2016.

507 Chen, C.-S., and Chen, Y.-L.: The Rainfall Characteristics of Taiwan, *Monthly Weather Review*,
508 131, 1323-1341, 10.1175/1520-0493(2003)131<1323:TRCOT>2.0.CO;2, 2003.

509 Chen, C.-S., Chen, Y.-L., Liu, C.-L., Lin, P.-L., and Chen, W.-C.: Statistics of Heavy Rainfall
 510 Occurrences in Taiwan, *Weather and Forecasting*, 22, 981-1002, 10.1175/waf1033.1, 2007.

511 Chen, G., Zhao, K., Zhang, G., Huang, H., Liu, S., Wen, L., Yang, Z., Yang, Z., Xu, L., and Zhu,
 512 W.: Improving Polarimetric C-Band Radar Rainfall Estimation with Two-Dimensional
 513 Video Disdrometer Observations in Eastern China, *Journal of Hydrometeorology*, 18,
 514 1375-1391, 10.1175/jhm-d-16-0215.1, 2017.

515 Chen, J.-M., Li, T., and Shih, C.-F.: Tropical Cyclone– and Monsoon-Induced Rainfall
 516 Variability in Taiwan, *Journal of Climate*, 23, 4107-4120, 10.1175/2010jcli3355.1, 2010.

517 Chen, J.-M., and Chen, H.-S.: Interdecadal Variability of Summer Rainfall in Taiwan Associated
 518 with Tropical Cyclones and Monsoon, *Journal of Climate*, 24, 5786-5798,
 519 10.1175/2011jcli4043.1, 2011.

520 Chen, K., Chu, C.-Y., and Tzeng, Y.-C.: A semi-empirical model of rain attenuation at Ka-band
 521 in Northern Taiwan, *Progress In Electromagnetics Research*, 16, 213-223, 2011.

522 Chen, T.-C., Yen, M.-C., Hsieh, J.-C., and Arritt, R. W.: Diurnal and Seasonal Variations of the
 523 Rainfall Measured by the Automatic Rainfall and Meteorological Telemetry System in
 524 Taiwan, *Bulletin of the American Meteorological Society*, 80, 2299-2312, 10.1175/1520-
 525 0477(1999)080<2299:DASVOT>2.0.CO;2, 1999.

526 Chen, Y., Duan, J., An, J., and Liu, H.: Raindrop Size Distribution Characteristics for Tropical
 527 Cyclones and Meiyu-Baiu Fronts Impacting Tokyo, Japan, *Atmosphere-Basel*, 10, 391,
 528 2019.

529 Chu, P.-S., Zhao, X., Lee, C.-T., and Lu, M.-M.: Climate prediction of tropical cyclone activity
 530 in the vicinity of Taiwan using the multivariate least absolute deviation regression method,
 531 Terrestrial Atmospheric and Oceanic Sciences, 18, 805, 2007.

532 Chu, Y.-H., and Su, C.-L.: An Investigation of the Slope–Shape Relation for Gamma Raindrop
 533 Size Distribution, Journal of Applied Meteorology and Climatology, 47, 2531-2544,
 534 10.1175/2008jamc1755.1, 2008.

535 Dee, D. P., Uppala, S., Simmons, A., Berrisford, P., Poli, P., Kobayashi, S., Andrae, U.,
 536 Balmaseda, M., Balsamo, G., and Bauer, d. P.: The ERA-Interim Reanalysis:
 537 Configuration and Performance of the Data Assimilation System, Quarterly Journal of the
 538 royal meteorological society, 137, 553-597, 2011.

539 Deo, A., and Walsh, K. J.: Contrasting tropical cyclone and non-tropical cyclone related rainfall
 540 drop size distribution at Darwin, Australia, Atmospheric Research, 181, 81-94, 2016.

541 Fornis, R. L., Vermeulen, H. R., and Nieuwenhuis, J. D.: Kinetic Energy–Rainfall Intensity
 542 Relationship For Central Cebu, Philippines for Soil Erosion Studies, Journal of
 543 Hydrology, 300, 20-32, 10.1016/j.jhydrol.2004.04.027, 2005.

544 Hu, Z., and Srivastava, R. C.: Evolution of Raindrop Size Distribution by Coalescence, Breakup,
 545 and Evaporation: Theory and Observations, Journal of the Atmospheric Sciences, 52,
 546 1761-1783, 10.1175/1520-0469(1995)052<1761:EORSDB>2.0.CO;2, 1995.

547 Iguchi, T., Kozu, T., Meneghini, R., Awaka, J., and Okamoto, K. i.: Rain-Profiling Algorithm for
548 the TRMM Precipitation Radar, Journal of Applied Meteorology, 39, 2038-2052,
549 10.1175/1520-0450(2001)040<2038:RPAFTT>2.0.CO;2, 2000.

550 Janapati, J., Reddy, V., Reddy, K., Lin, P.-L., and Liu, C.-Y.: A study on raindrop size
551 distribution variability in before and after landfall precipitations of tropical cyclones
552 observed over southern India, Journal of Atmospheric and Solar-Terrestrial Physics, 159,
553 23-40, 2017.

554 Janapati, J., Seela, B. K., Lin, P.-L., Wang, P. K., and Kumar, U.: An assessment of tropical
555 cyclones rainfall erosivity for taiwan, Scientific reports, 9, 15862, 2019.

556 Janapati, J., Seela, B. K., Lin, P.-L., Wang, P. K., Tseng, C.-H., Reddy, K. K., Hashiguchi, H.,
557 Feng, L., Das, S. K., and Unnikrishnan, C. K.: Raindrop Size Distribution Characteristics
558 of Indian and Pacific Ocean Tropical Cyclones Observed at India and Taiwan Sites,
559 Journal of the Meteorological Society of Japan. Ser. II, 98, 299-317, 10.2151/jmsj.2020-
560 015, 2020.

561 Jayalakshmi, J., and Reddy, K. K.: Raindrop size distributions of southwest and northeast
562 monsoon heavy precipitation observed over Kadapa (14°4'N, 78°82'E), a semi-arid region
563 of India, Current Science, 107, 1312-1320, 2014.

564 Joss, J., and Waldvogel, A.: Raindrop Size Distribution and Sampling Size Errors, Journal of the
565 Atmospheric Sciences, 26, 566-569, 10.1175/1520-
566 0469(1969)026<0566:RSDASS>2.0.CO;2, 1969.

567 Jung, S.-A., Lee, D.-I., Jou, B. J.-D., and Uyeda, H.: Microphysical Properties of Maritime
568 Squall Line Observed on June 2, 2008 in Taiwan, Journal of the Meteorological Society of
569 Japan. Ser. II, 90, 833-850, 10.2151/jmsj.2012-516, 2012.

570 Kinnell, P. I. A.: Rainfall Intensity-Kinetic Energy Relationships for Soil Loss Prediction1, Soil
571 Science Society of America Journal, 45, 153-155,
572 10.2136/sssaj1981.03615995004500010033x, 1981.

573 Krishna, U. V. M., Reddy, K. K., Seela, B. K., Shirooka, R., Lin, P.-L., and Pan, C.-J.: Raindrop
574 size distribution of easterly and westerly monsoon precipitation observed over Palau
575 islands in the Western Pacific Ocean, Atmospheric Research, 174-175, 41-51,
576 <https://doi.org/10.1016/j.atmosres.2016.01.013>, 2016.

577 Kumar, S. B., and Reddy, K. K.: Rain drop size distribution characteristics of cyclonic and north
578 east monsoon thunderstorm precipitating clouds observed over Kadapa (14.47°N,
579 78.82°E), tropical semi-arid region of India, Mausam, 64, 35–48, 2013.

580 Kumari, N., Kumar, S. B., Jayalakshmi, J., and Reddy, K. K.: Raindrop size distribution
581 variations in JAL and NILAM cyclones induced precipitation observed over Kadapa
582 (14.47 o N, 78.82 o E), a tropical semi-arid region of India, Indian Journal of Radio and
583 Space Physics, 43, 57–66, 2014.

584 Kummerow, C., Hong, Y., Olson, W. S., Yang, S., Adler, R. F., McCollum, J., Ferraro, R., Petty,
585 G., Shin, D. B., and Wilheit, T. T.: The Evolution of the Goddard Profiling Algorithm
586 (GPROF) for Rainfall Estimation from Passive Microwave Sensors, Journal of Applied

587 Meteorology, 40, 1801-1820, 10.1175/1520-0450(2001)040<1801:TEOTGP>2.0.CO;2,
588 2001.

589 Lee, G. W., and Zawadzki, I.: Variability of Drop Size Distributions: Noise and Noise Filtering
590 in Disdrometric Data, Journal of Applied Meteorology, 44, 634-652, 10.1175/JAM2222.1,
591 2005.

592 Lee, M.-T., Lin, P.-L., Chang, W.-Y., Seela, B. K., and Janapati, J.: Microphysical
593 Characteristics and Types of Precipitation for Different Seasons over North Taiwan,
594 Journal of the Meteorological Society of Japan. Ser. II, 97, 841-865, 10.2151/jmsj.2019-
595 048, 2019.

596 Liang, A., Oey, L., Huang, S., and Chou, S.: Long-term trends of typhoon-induced rainfall over
597 Taiwan: In situ evidence of poleward shift of typhoons in western North Pacific in recent
598 decades, Journal of Geophysical Research: Atmospheres, 122, 2750-2765,
599 10.1002/2017jd026446, 2017.

600 Liao, L., Meneghini, R., and Tokay, A.: Uncertainties of GPM DPR Rain Estimates Caused by
601 DSD Parameterizations, Journal of Applied Meteorology and Climatology, 53, 2524-2537,
602 10.1175/JAMC-D-14-0003.1, 2014.

603 Lin, G.-W., and Chen, H.: The relationship of rainfall energy with landslides and sediment
604 delivery, Engineering geology, 125, 108-118, 2012.

605 Lu, J.-Y., Su, C.-C., Lu, T.-F., and Maa, M.-M.: Number and volume raindrop size distributions
606 in Taiwan, Hydrological Processes, 22, 2148-2158, 10.1002/hyp.6814, 2008.

607 Ma, Y., Ni, G., Chandra, C. V., Tian, F., and Chen, H.: Statistical characteristics of raindrop size
608 distribution during rainy seasons in the Beijing urban area and implications for radar
609 rainfall estimation, *Hydrology and Earth System Sciences*, 23, 4153-4170, 2019.

610 Maki, M., Keenan, T. D., Sasaki, Y., and Nakamura, K.: Characteristics of the Raindrop Size
611 Distribution in Tropical Continental Squall Lines Observed in Darwin, Australia, *Journal*
612 *of Applied Meteorology*, 40, 1393-1412, 10.1175/1520-
613 0450(2001)040<1393:COTRSD>2.0.CO;2, 2001.

614 McFarquhar, G. M., and List, R.: The Effect of Curve Fits for the Disdrometer Calibration on
615 Raindrop Spectra, Rainfall Rate, and Radar Reflectivity, *Journal of Applied Meteorology*,
616 32, 774-782, 10.1175/1520-0450(1993)032<0774:TEOCFF>2.0.CO;2, 1993.

617 McFarquhar, G. M., Hsieh, T.-L., Freer, M., Mascio, J., and Jewett, B. F.: The characterization
618 of ice hydrometeor gamma size distributions as volumes in $N_0-\lambda-\mu$ phase space:
619 Implications for microphysical process modeling, *Journal of the Atmospheric Sciences*, 72,
620 892-909, 2015.

621 Nakajima, T., and King, M. D.: Determination of the Optical Thickness and Effective Particle
622 Radius of Clouds from Reflected Solar Radiation Measurements. Part I: Theory, *Journal of*
623 *the Atmospheric Sciences*, 47, 1878-1893, 10.1175/1520-
624 0469(1990)047<1878:DOTOTA>2.0.CO;2, 1989.

625 Nakamura, K., and Iguchi, T.: Dual-wavelength Radar Algorithm, in: *Measuring precipitation*
626 *from space*, Springer, 225-234, 2007.

627 Platnick, S., King, M., and Hubanks, P.: MODIS Atmosphere L3 Daily Product, NASA MODIS
628 Adaptive Processing System, Goddard Space Flight Center, in, 2015.

629 Radhakrishna, B., and Narayana Rao, T.: Differences in cyclonic raindrop size distribution from
630 southwest to northeast monsoon season and from that of noncyclonic rain, *Journal of*
631 *Geophysical Research: Atmospheres*, 115, 10.1029/2009jd013355, 2010.

632 Remer, L. A., Kaufman, Y. J., Tanré, D., Mattoo, S., Chu, D. A., Martins, J. V., Li, R. R.,
633 Ichoku, C., Levy, R. C., Kleidman, R. G., Eck, T. F., Vermote, E., and Holben, B. N.: The
634 MODIS Aerosol Algorithm, Products, and Validation, *Journal of the Atmospheric*
635 *Sciences*, 62, 947-973, 10.1175/JAS3385.1, 2005.

636 Renard, K. G., Foster, G. R., Weesies, G. A., McCool, D. K., and Yoder, D. C.: Predicting Soil
637 Erosion by Water: A Guide to Conservation Planning with the Revised Universal Soil Loss
638 Equation (RUSLE) (Agricultural Handbook 703). US Department of Agriculture,
639 Washington, DC., 1997.

640 Rosenfeld, D., and Ulbrich, C. W.: Cloud Microphysical Properties, Processes, and Rainfall
641 Estimation Opportunities, *Meteorological Monographs*, 52, 237-258, 10.1175/0065-
642 9401(2003)030<0237:CMPPAR>2.0.CO;2, 2003.

643 Ryzhkov, A. V., and Zrnić, D. S.: Comparison of Dual-Polarization Radar Estimators of Rain,
644 *Journal of Atmospheric and Oceanic Technology*, 12, 249-256, 10.1175/1520-
645 0426(1995)012<0249:CODPRE>2.0.CO;2, 1995.

646 Salles, C., Poesen, J., and Sempere-Torres, D.: Kinetic Energy of Rain and Its Functional
647 Relationship With Intensity, *Journal of Hydrology*, 257, 256-270, 10.1016/S0022-
648 1694(01)00555-8, 2002.

649 Sauvageot, H., and Lacaux, J.-P.: The Shape of Averaged Drop Size Distributions, *Journal of the*
650 *Atmospheric Sciences*, 52, 1070-1083, 10.1175/1520-
651 0469(1995)052<1070:TSOADS>2.0.CO;2, 1995.

652 Seela, B. K., Reddy, K. K., Jayalakshmi, J., Rao, T. N., Lin, P.-L., Liu, C.-Y., and Kumar, U.:
653 Precipitation and cloud microstructure variations between two southern Indian stations,
654 *Remote Sensing of the Atmosphere, Clouds, and Precipitation VI*, 2016, 98761O,

655 Seela, B. K., Janapati, J., Lin, P.-L., Reddy, K. K., Shirooka, R., and Wang, P. K.: A Comparison
656 Study of Summer Season Raindrop Size Distribution Between Palau and Taiwan, Two
657 Islands in Western Pacific, *Journal of Geophysical Research: Atmospheres*, 122, 11,787-
658 711,805, 10.1002/2017jd026816, 2017.

659 Seela, B. K., Janapati, J., Lin, P.-L., Wang, P. K., and Lee, M.-T.: Raindrop Size Distribution
660 Characteristics of Summer and Winter Season Rainfall Over North Taiwan, *Journal of*
661 *Geophysical Research: Atmospheres*, 123, 11,602-611,624, 10.1029/2018jd028307, 2018.

662 Sheppard, B. E.: Effect of Irregularities in the Diameter Classification of Raindrops by the Joss-
663 Waldvogel Disdrometer, *Journal of Atmospheric and Oceanic Technology*, 7, 180-183,
664 10.1175/1520-0426(1990)007<0180:EOIITD>2.0.CO;2, 1990.

665 Sheppard, B. E., and Joe, P. I.: Comparison of Raindrop Size Distribution Measurements by a
 666 Joss-Waldvogel Disdrometer, a PMS 2DG Spectrometer, and a POSS Doppler Radar,
 667 Journal of Atmospheric and Oceanic Technology, 11, 874-887, 10.1175/1520-
 668 0426(1994)011<0874:CORSDM>2.0.CO;2, 1994.

669 Steiner, M., Smith, J. A., and Uijlenhoet, R.: A Microphysical Interpretation of Radar
 670 Reflectivity–Rain Rate Relationships, Journal of the Atmospheric Sciences, 61, 1114-1131,
 671 10.1175/1520-0469(2004)061<1114:Amiorr>2.0.Co;2, 2004.

672 Testud, J., Oury, S., Black, R. A., Amayenc, P., and Dou, X.: The Concept of “Normalized”
 673 Distribution to Describe Raindrop Spectra: A Tool for Cloud Physics and Cloud Remote
 674 Sensing, Journal of Applied Meteorology, 40, 1118-1140, 10.1175/1520-
 675 0450(2001)040<1118:TCOND>2.0.CO;2, 2001.

676 Thompson, E. J., Rutledge, S. A., Dolan, B., and Thurai, M.: Drop Size Distributions and Radar
 677 Observations of Convective and Stratiform Rain over the Equatorial Indian and West
 678 Pacific Oceans, Journal of the Atmospheric Sciences, 72, 4091-4125, 10.1175/JAS-D-14-
 679 0206.1, 2015.

680 Tokay, A., and Short, D. A.: Evidence from Tropical Raindrop Spectra of the Origin of Rain
 681 from Stratiform versus Convective Clouds, Journal of Applied Meteorology, 35, 355-371,
 682 10.1175/1520-0450(1996)035<0355:Efterso>2.0.Co;2, 1996.

683 Tokay, A., Kruger, A., and Krajewski, W. F.: Comparison of Drop Size Distribution
 684 Measurements by Impact and Optical Disdrometers, Journal of Applied Meteorology, 40,
 685 2083-2097, 10.1175/1520-0450(2001)040<2083:CODSDM>2.0.CO;2, 2001.

686 Tokay, A., Bashor, P. G., Habib, E., and Kasparis, T.: Raindrop Size Distribution Measurements
687 in Tropical Cyclones, *Monthly Weather Review*, 136, 1669-1685,
688 10.1175/2007mwr2122.1, 2008.

689 Tokay, A., Petersen, W. A., Gatlin, P., and Wingo, M.: Comparison of Raindrop Size
690 Distribution Measurements by Collocated Disdrometers, *Journal of Atmospheric and*
691 *Oceanic Technology*, 30, 1672-1690, 10.1175/JTECH-D-12-00163.1, 2013.

692 Tu, J.-Y., and Chou, C.: Changes in precipitation frequency and intensity in the vicinity of
693 Taiwan: typhoon versus non-typhoon events, *Environmental Research Letters*, 8, 014023,
694 10.1088/1748-9326/8/1/014023, 2013.

695 Ulbrich, C. W., and Atlas, D.: Microphysics of Raindrop Size Spectra: Tropical Continental and
696 Maritime Storms, *Journal of Applied Meteorology and Climatology*, 46, 1777-1791,
697 10.1175/2007JAMC1649.1, 2007.

698 van Dijk, A. I. J. M., Bruijnzeel, L. A., and Rosewell, C. J.: Rainfall Intensity–Kinetic Energy
699 Relationships: A Critical Literature Appraisal, *Journal of Hydrology*, 261, 1-23,
700 10.1016/S0022-1694(02)00020-3, 2002.

701 Wen, L., Zhao, K., Chen, G., Wang, M., Zhou, B., Huang, H., Hu, D., Lee, W.-C., and Hu, H.:
702 Drop size distribution characteristics of seven typhoons in China, *J. Geophys. Res. Atmos.*,
703 123, 6529–6548, doi:10.1029/2017JD027950, 2018.

704 Wen, L., Zhao, K., Wang, M., and Zhang, G.: Seasonal Variations of Observed Raindrop Size
705 Distribution in East China, *Advances in Atmospheric Sciences*, 36, 346-362, 2019.

706 Wischmeier, W. H.: A Rainfall Erosion Index for a Universal Soil-Loss Equation¹, Soil Science
707 Society of America Journal, 23, 246-249, 10.2136/sssaj1959.03615995002300030027x,
708 1959.

709 Wu, Z., Zhang, Y., Zhang, L., Lei, H., Xie, Y., Wen, L., and Yang, J.: Characteristics of summer
710 season raindrop size distribution in three typical regions of western Pacific, Journal of
711 Geophysical Research: Atmospheres, 124, 4054-4073, 2019.

712 Zhang, Y., Liu, L., Bi, S., Wu, Z., Shen, P., Ao, Z., Chen, C., and Zhang, Y.: Analysis of dual-
713 polarimetric radar variables and quantitative precipitation estimators for landfall typhoons
714 and squall lines based on disdrometer data in southern China, Atmosphere, 10, 30, 2019.

715

716

Table 1. The JWD and rain gauge comparison results (n: number of rainy days, CC: correlation coefficient, RMSE: root mean square error) for different wind speed conditions (daily maximum wind speed: 0-8, 8-14, 14-18, > 18 m s⁻¹). Note: there were no NTY rainy days with daily maximum wind speed > 14 m s⁻¹.

Wind speed (m s ⁻¹)	TY			NTY		
	n	CC	RMSE (mm)	n	CC	RMSE (mm)
0-8	21	0.989	6.305	113	0.956	3.853
8-14	27	0.99	5.153	18	0.942	3.482
14-18	8	0.953	18.112	-	-	-
>18	3	0.996	7.448	-	-	-

729

730 **Table 2.** Rainy minutes (N), mean, standard deviation (Std), Skewness and Kurtosis of seven
 731 rainfall rate classes for typhoon (TY) and non-typhoon (NTY) rainy days of summer
 732 seasons.

Rain rate class	Rain rate threshold (mm h ⁻¹)	Typhoon (TY)					non-typhoon (NTY)				
		No. of sampl es	Mean (mm h ⁻¹)	Stand ard deviat ion (mm h ⁻¹)	Ske wnes s	Kurto sis	No. of sampl es	Mean (mm h ⁻¹)	Stand ard deviat ion (mm h ⁻¹)	Skew ness	Kurt osis
C1	$0.1 \leq R < 1$	9317	0.43	0.26	0.55	2.1	10661	0.4	0.25	0.71	2.34
C2	$1 \leq R < 2$	3274	1.44	0.29	0.24	1.84	3193	1.43	0.29	0.29	1.88
C3	$2 \leq R < 5$	4747	3.29	0.85	0.31	1.92	3404	3.17	0.83	0.46	2.1
C4	$5 \leq R < 10$	2799	7	1.4	0.43	2.04	1404	6.98	1.42	0.43	2.01
C5	$10 \leq R < 30$	2313	16.44	5.24	0.77	2.59	1234	17.46	5.6	0.5	2.08
C6	$30 \leq R < 50$	393	38.31	5.73	0.37	1.92	320	37.88	5.67	0.45	2.01
C7	$R > 50$	231	67.15	14.91	1.16	3.97	152	65.86	14.94	1.51	5.18
total		23074	4.88	9.38	4.59	31.51	20368	3.59	8.38	5.2	38.9

733

734

Table 3. Statistical parameters [correlation coefficient: R^2 , Root mean square error (RMSE), normalized RMSE] for typhoon (TY) and non-typhoon (NTY) rainy days. **Note:** Units for RMSE are $J m^{-2} h^{-1}$ for $KE_{time}-R$ relations and $J m^{-2} mm^{-1}$ for $KE_{mm}-R$ and $KE_{mm}-D_m$ relations.

Weather condition	Statistical parameter	$KE_{time}-R$		$KE_{mm}-R$			$KE_{mm}-D_m$
		Linear	Power	Power	Exp	Log	Second order polynomial
TY	R^2	0.986	0.994	0.694	0.68	0.68	0.992
	RMSE	37.488	24.785	3.973	10.227	4.047	12.396
	NRMSE	0.306	0.202	0.032	0.083	0.033	2.514
NTY	R^2	0.984	0.99	0.646	0.639	0.639	0.988
	RMSE	38.012	30.745	4.599	11.017	4.636	12.93
	NRMSE	0.322	0.26	0.039	0.093	0.039	2.803

Figures

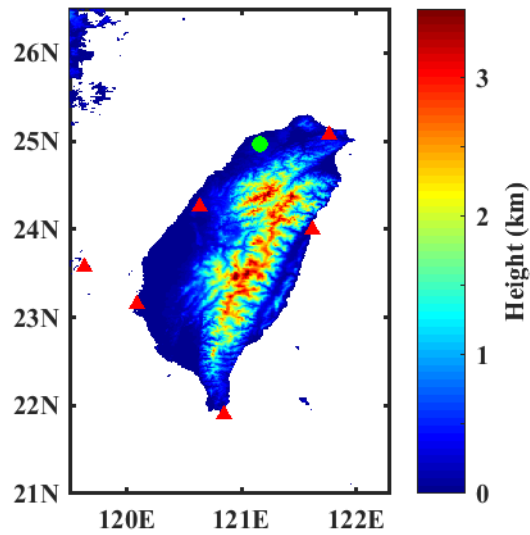


Figure 1. Map of Taiwan with disdrometer (green color circle) and radars (red color triangles) sites.

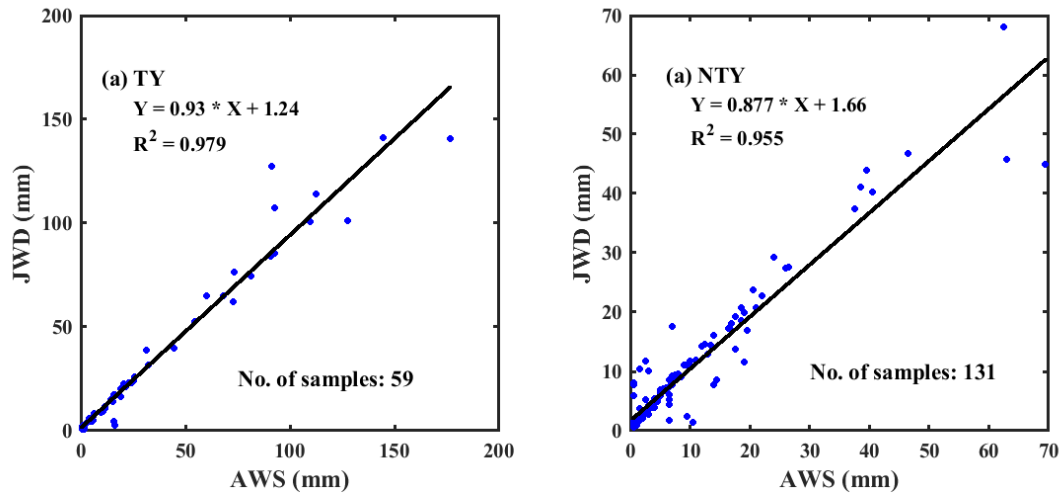
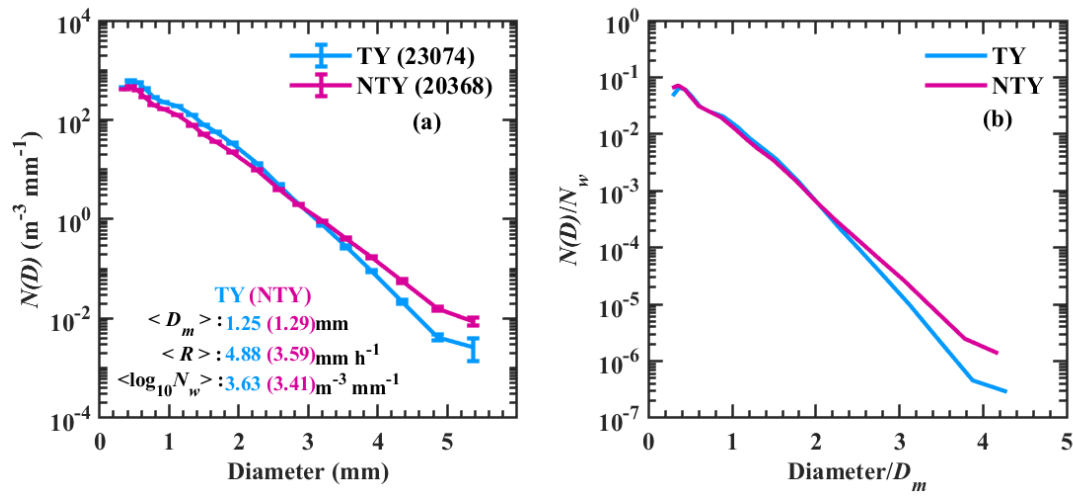


Figure 2. The JWD and rain gauge daily accumulations scatter plot for (a) typhoon (TY) and (b) non-typhoon (NTY) rainfall.

768



769

770 **Figure 3.** (a) Distributions of mean concentration [$N(D)$, in $\text{mm}^{-1} \text{m}^{-3}$] with raindrop diameter
 771 for typhoon (TY) and non-typhoon (NTY) rainfall and their (b) normalized spectra.

772

773

774

775

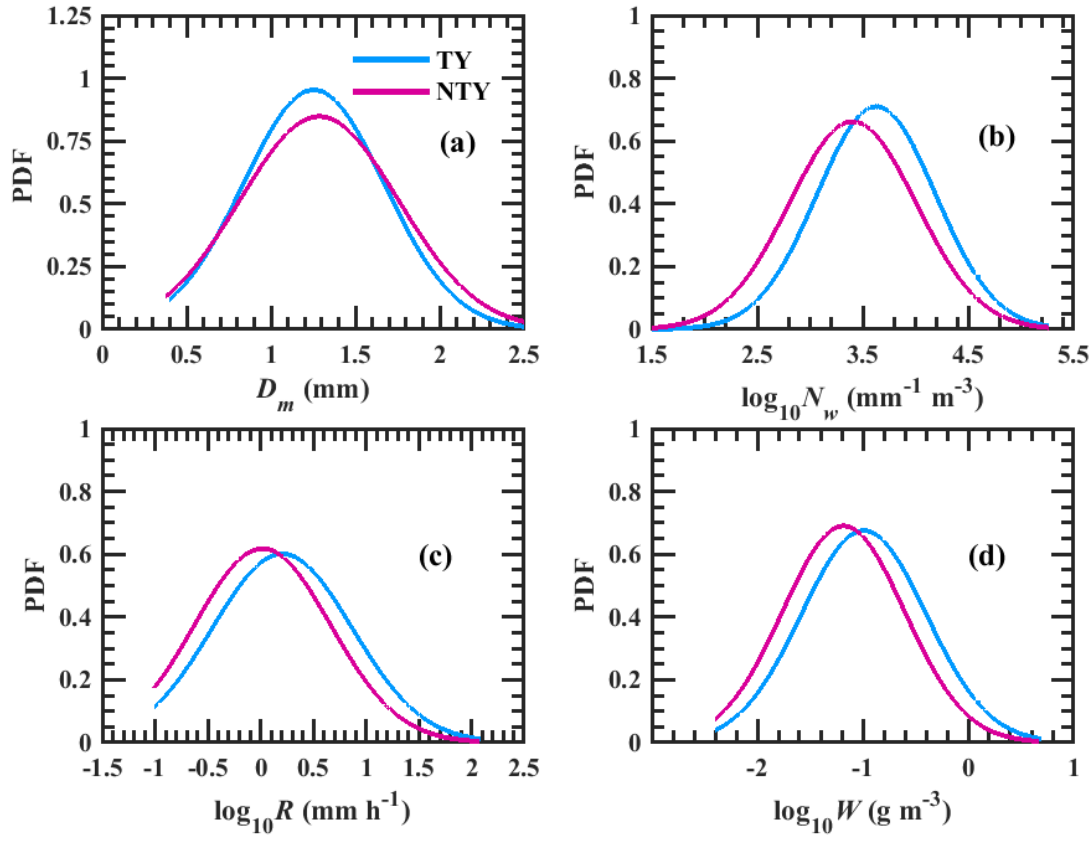


Figure 4. The probability distribution functions (PDF) of (a) mass-weighted mean diameter, D_m (mm), (b) $\log_{10} N_w$ (N_w is the normalized intercept parameter in $\text{mm}^{-1} \text{m}^{-3}$), (c) $\log_{10} R$ (R is rainfall rate in mm h^{-1}), and (d) $\log_{10} W$ (W is the liquid water content in g m^{-3}) for typhoon (TY) and non-typhoon (NTY) rainfall.

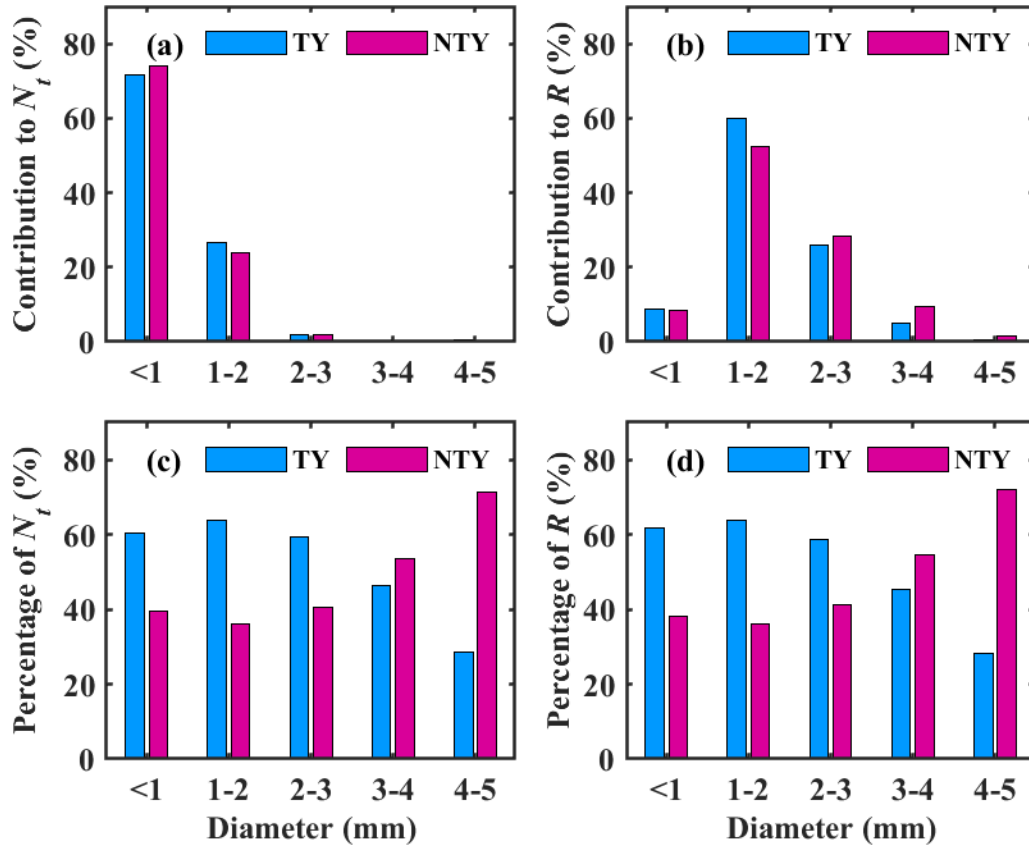


Figure 5. Contribution of drop diameter classes (Diameter < 1 mm, 1–2 mm, 2–3 mm, 3–4 mm, and 4–5 mm) to (a) total number concentration N_t (m^{-3}) and (b) rainfall rate R (mm h^{-1}) in typhoon (TY) and non-typhoon (NTY) rainfall. Occurrence percentage of (c) total number concentration N_t (m^{-3}) and (d) rainfall rate R (mm h^{-1}) in each diameter class for typhoon (TY) and non-typhoon (NTY) rainfall.

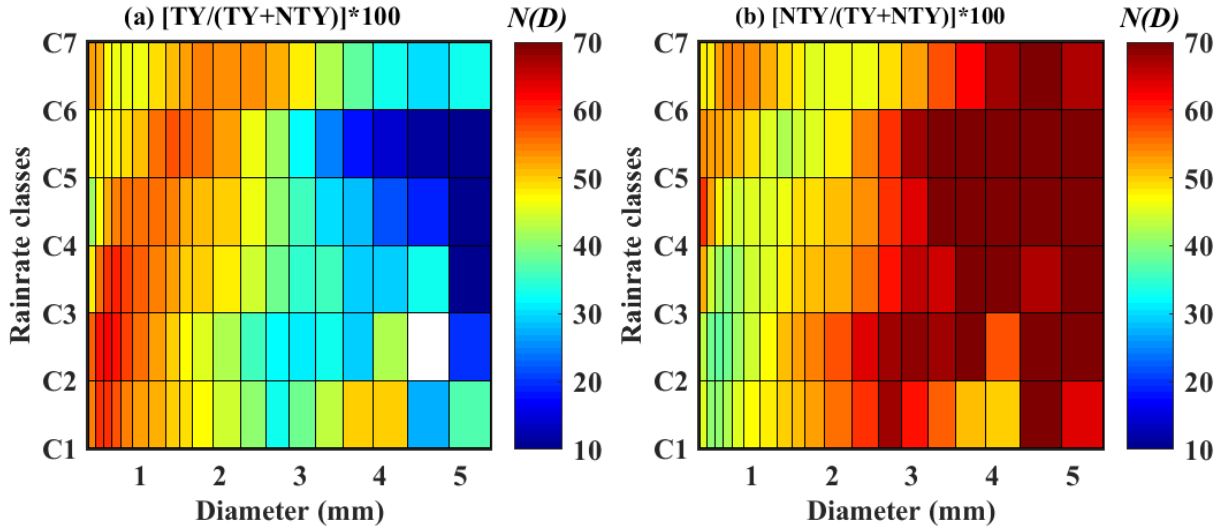


Figure 6 Percentage contribution of $N(D)$ ($\text{mm}^{-1} \text{m}^{-3}$) in different rainfall rate classes for typhoon (TY) and non-typhoon (NTY) rainfall.

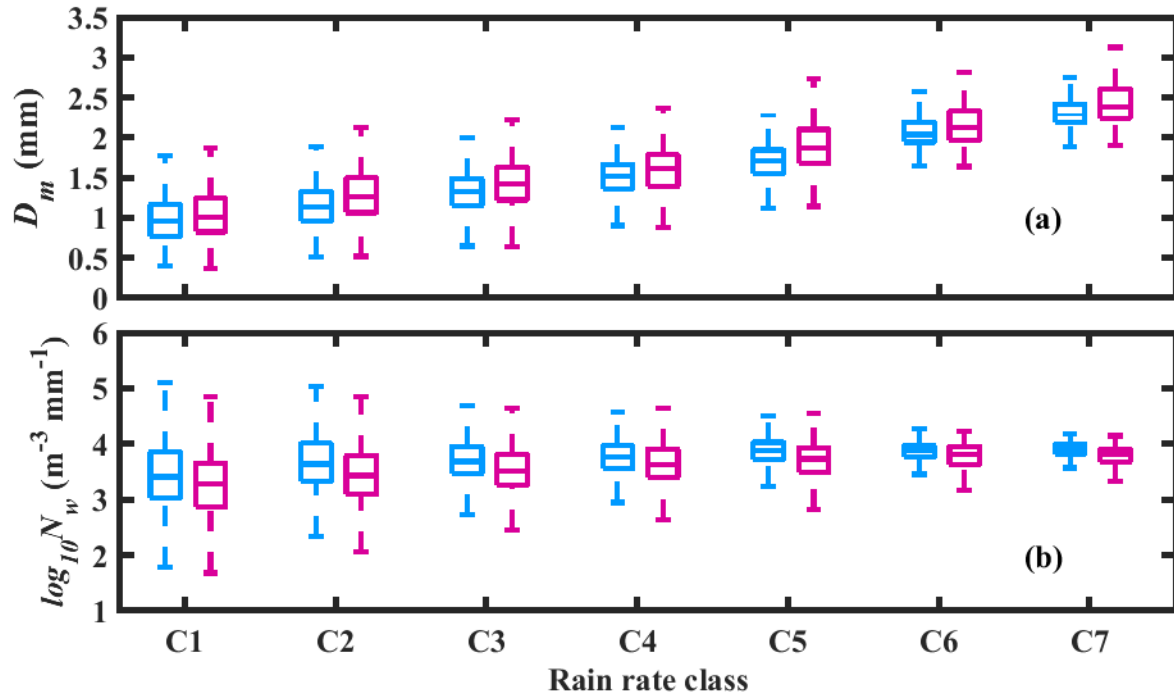


Figure 7. Box plot of (a) D_m (mm) and (b) $\log_{10} N_w$ ($\text{mm}^{-1} \text{m}^{-3}$) in seven rainfall rate classes for typhoon (TY) (sky blue color) and non-typhoon (NTY) (dark magenta color) rainfall. The center line of the box indicates the median, and the bottom and top lines of the box indicate the 25th and 75th percentiles, respectively. The bottom and top of the dashed vertical lines indicate the 5th and 95th percentiles, respectively.

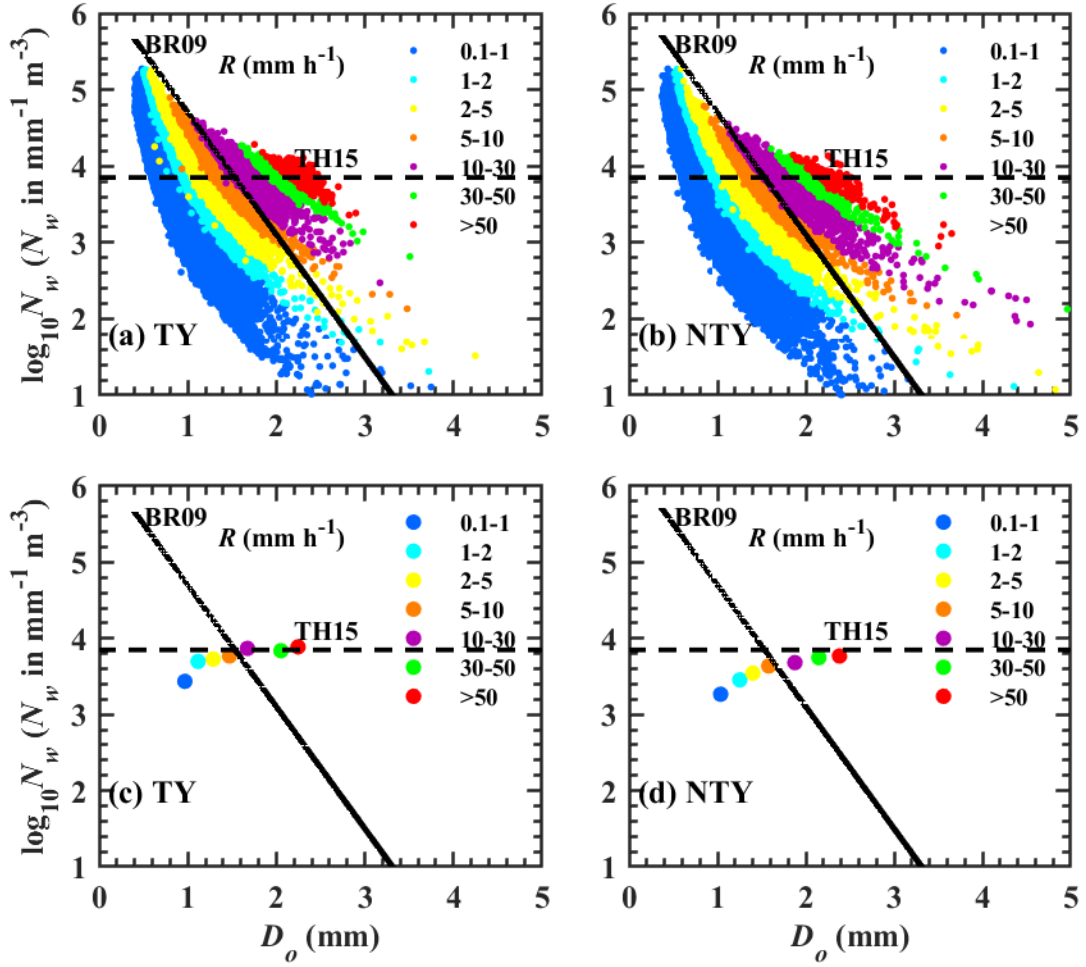


Figure 8. Scatter plots of D_0 - $\log_{10}N_w$ for (a) typhoon (TY) and (b) non-typhoon (NTY) rainfall, mean values of D_0 and $\log_{10}N_w$ for (c) typhoon (TY) and (d) non-typhoon (NTY) rainfall in different rainfall rate ranges. Stratiform and convective precipitation separation line of Thompson et al. (2015): TH15 and Bringi et al. (2009): BR09 are represented, respectively, with horizontal dotted line and inclined solid line.

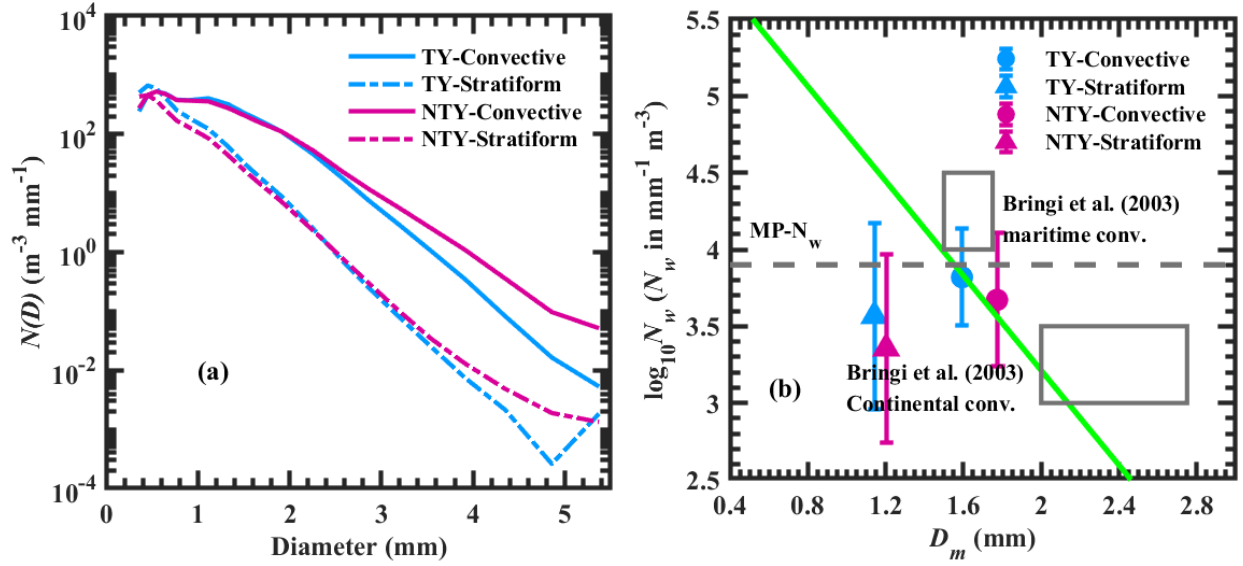
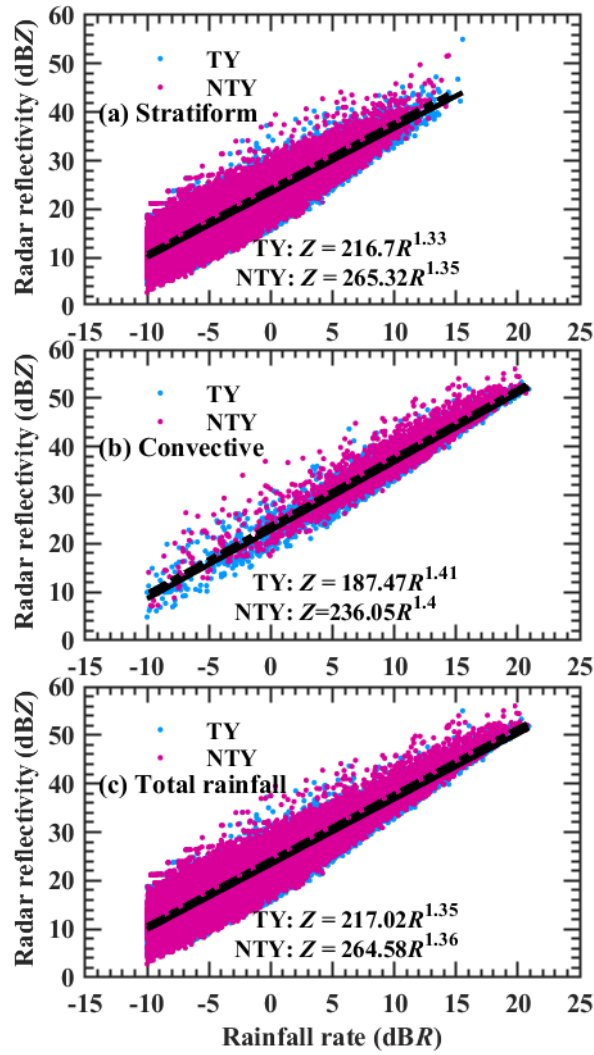


Figure 9. (a) Distribution of $N(D)$ ($\text{m}^{-3} \text{mm}^{-1}$) with raindrop diameter in stratiform and convective precipitation for typhoon (TY) and non-typhoon (NTY) rainfall. (b) Variations of $\log_{10} N_w$ (where N_w is the normalized intercept parameter in $\text{mm}^{-1} \text{m}^{-3}$) with D_m (mass-weighted mean diameter in mm) in stratiform and convective regimes for typhoon (TY) and non-typhoon (NTY) rainfall. The horizontal gray dashed line is the Marshall-Palmer value of $\log_{10} N_w$ (3.9) for exponential shape. The green dash dotted line is the stratiform and convective separation line of Bring et al. (2003).



822

823 **Figure 10.** Scatter plots of radar reflectivity (Z , dBZ) and rainfall rate in logarithmic scale

824 $(10 \cdot \log_{10} R, \text{dBR}, R \text{ in } \text{mm h}^{-1})$ for typhoon (TY) and non-typhoon (NTY) rainfall.

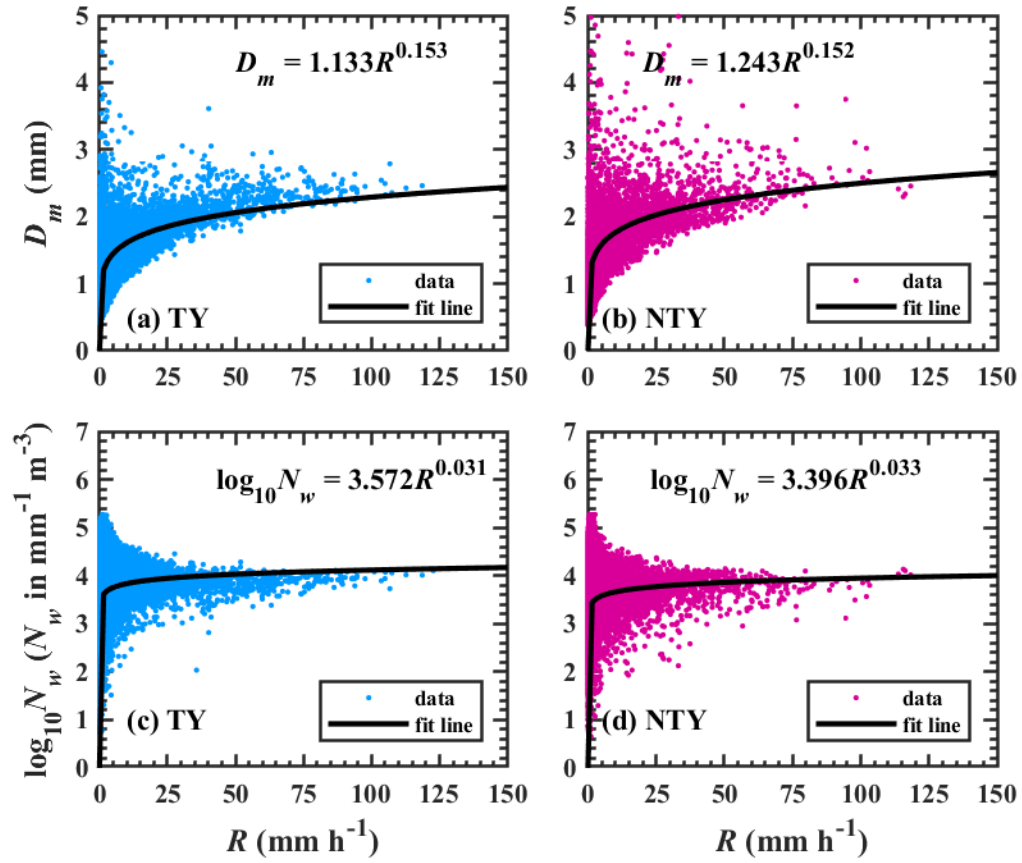


Figure 11. Distributions of D_m (mm) and $\log_{10}N_w$ (N_w in $\text{mm}^{-1} \text{m}^{-3}$) with rainfall rate (R , mm h^{-1}) for typhoon ([ENREF 31](#)TY) and non-typhoon (NTY) rainfall.

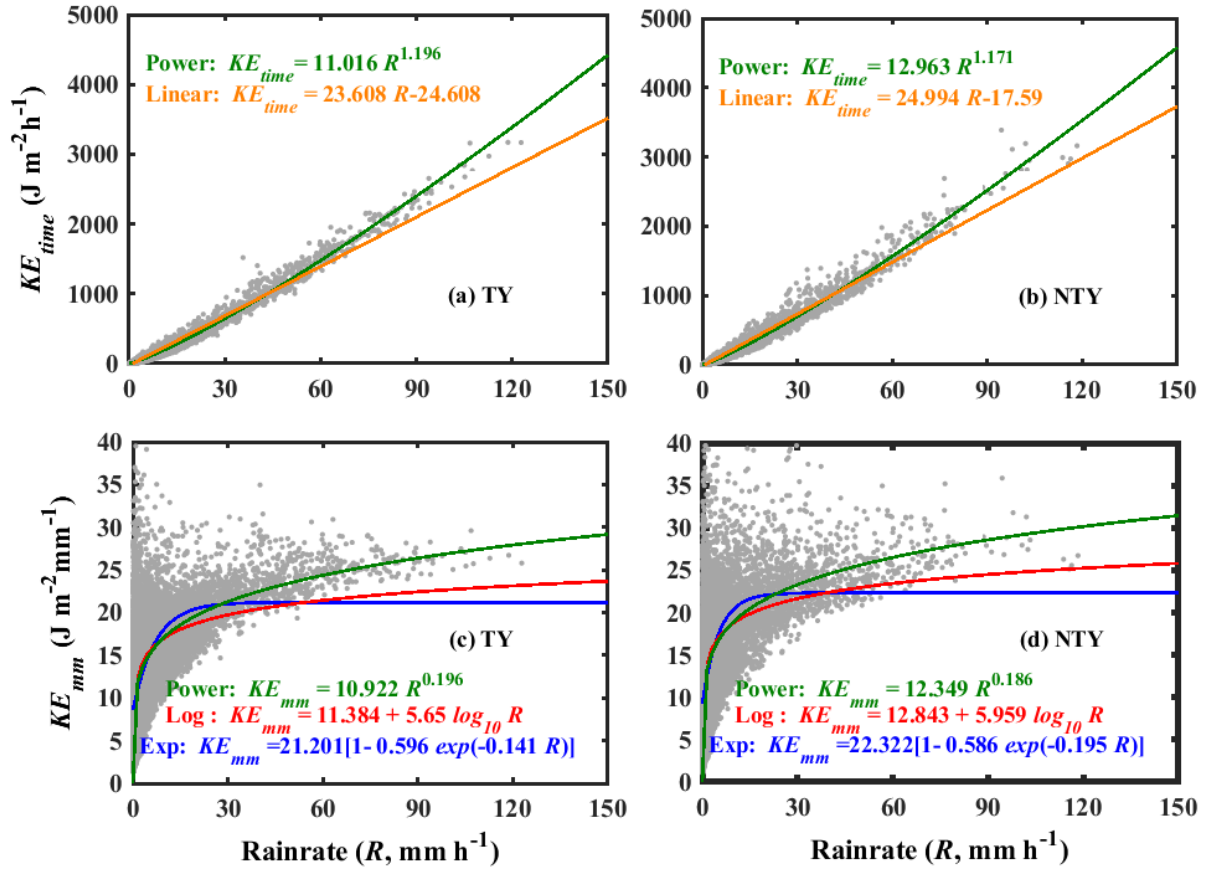
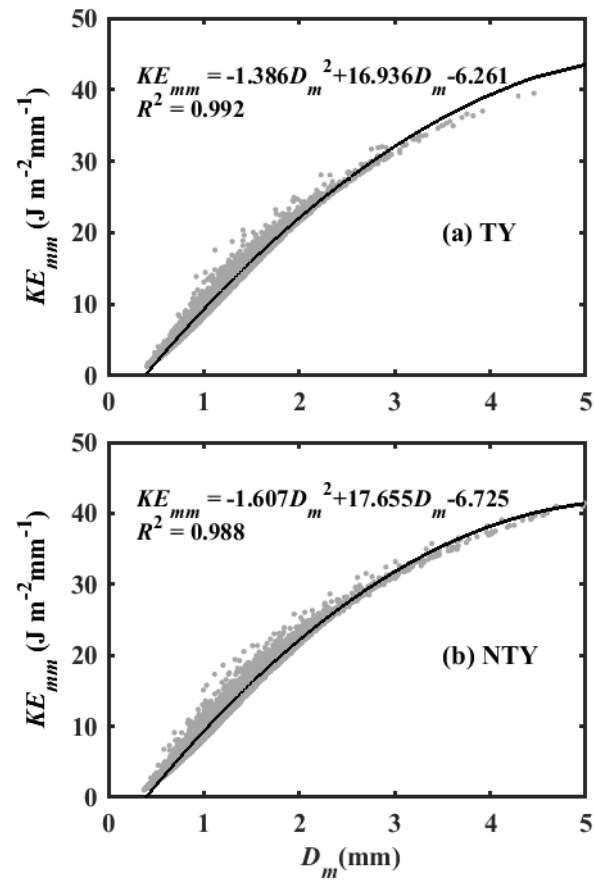


Figure 12. Scatter plots of rainfall kinetic energy (KE) [time-specific KE , KE_{time} ; volume-specific KE , KE_{mm}] with rainfall rate (R , mm h^{-1}) for typhoon (TY) and non-typhoon (NTY) rainfall.

842



843

844 **Figure 13.** Scatter plots of volume-specific KE (KE_{mm} in J m⁻² mm⁻¹) with D_m (mm) for typhoon
 845 (TY) and non-typhoon (NTY) rainfall.

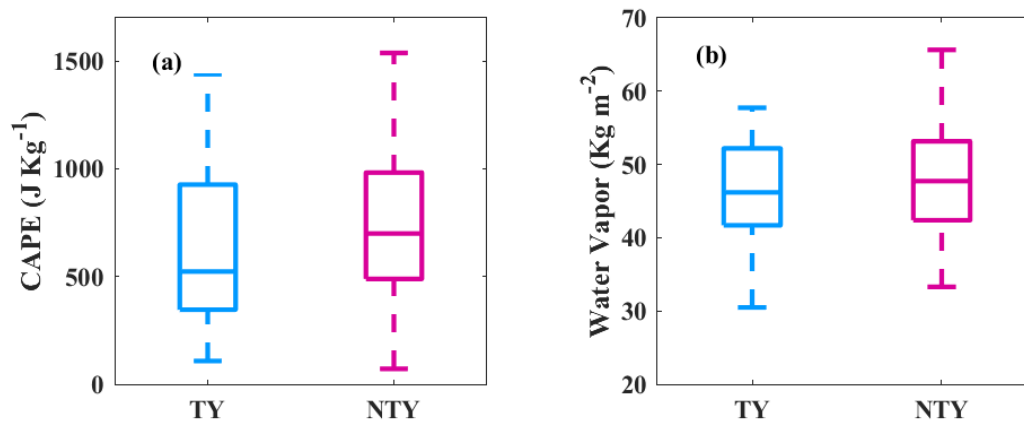
846

847

848

849

850



851

852 **Figure 14:** Variations in (a) convective available potential energy (CAPE, J Kg^{-1}) and (b)
853 vertical integral of water vapor (kg m^{-2}) for typhoon (TY) and non-typhoon (NTY)
854 rainfall. The center line of the box indicates the median, and the bottom and top lines of
855 the box indicate the 25th and 75th percentiles, respectively. The bottom and top of the
856 dashed vertical lines indicate the 5th and 95th percentiles, respectively

857

858

859

860

861

862

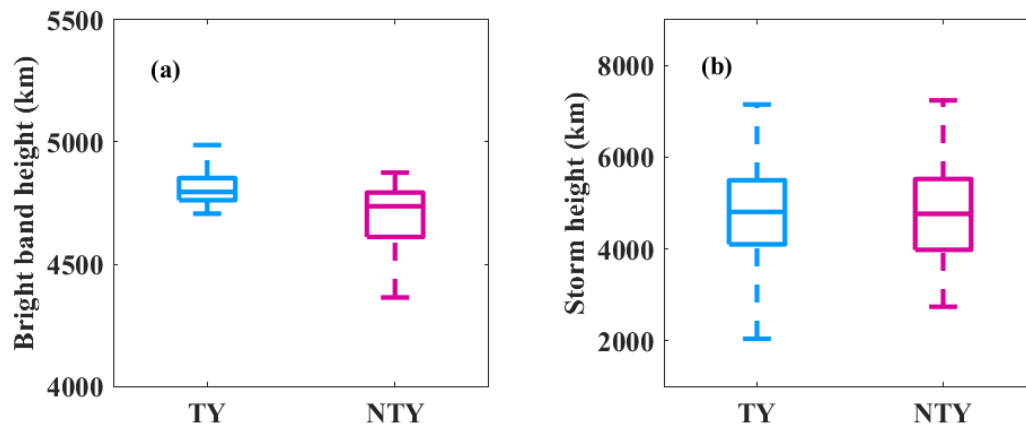


Figure 15. (a) Bright band (BB) and (b) storm heights box plots for typhoon (TY) and non-typhoon (NTY) rainfall.

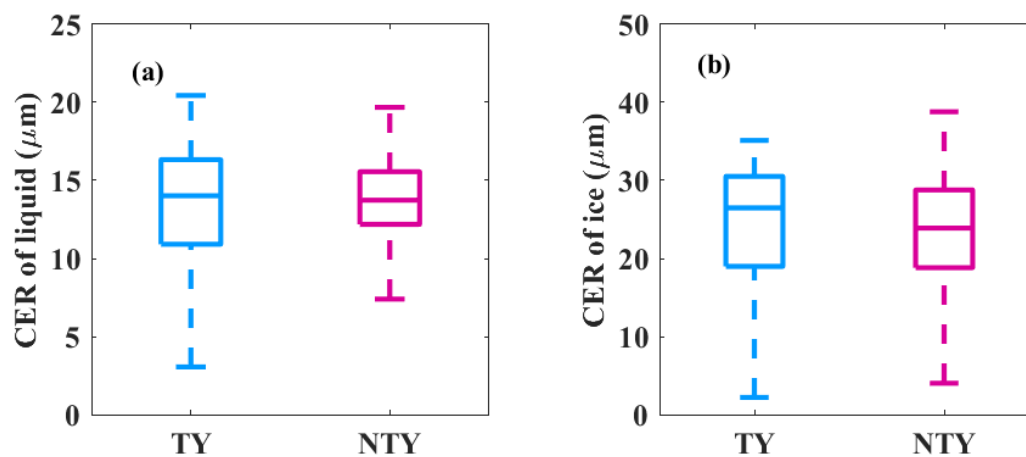


Figure 16. (a) Liquid, (b) ice particles cloud effective radii (CER, μm) values for typhoon (TY) and non-typhoon (NTY) rainfall.

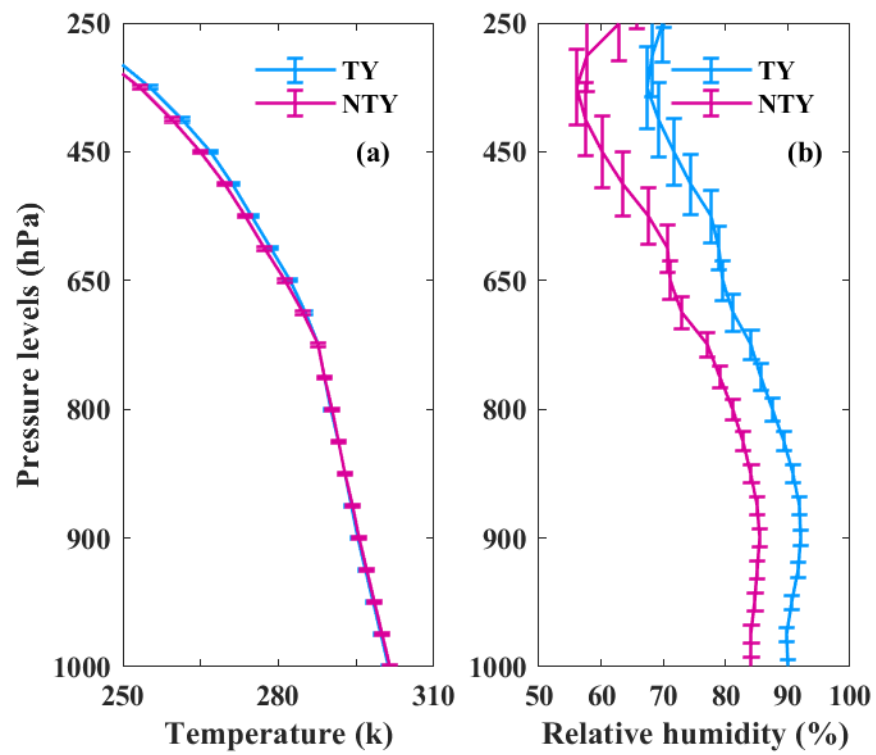


Figure 17. (a) Mean air temperature (°C) and (b) relative humidity (%) profiles for typhoon (TY) and non-typhoon (NTY) rainfall.

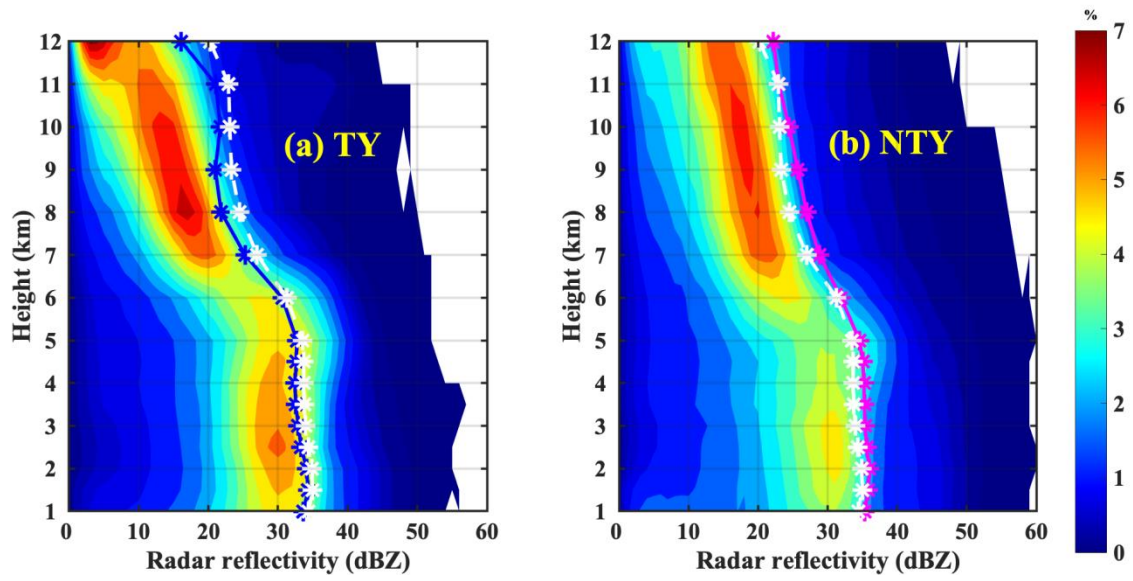


Figure 18. Radar reflectivity contoured frequency-by-altitude diagram (CFAD) from six ground-based radars for (a) typhoon (TY) and (b) non-typhoon (NTY) rainfall.

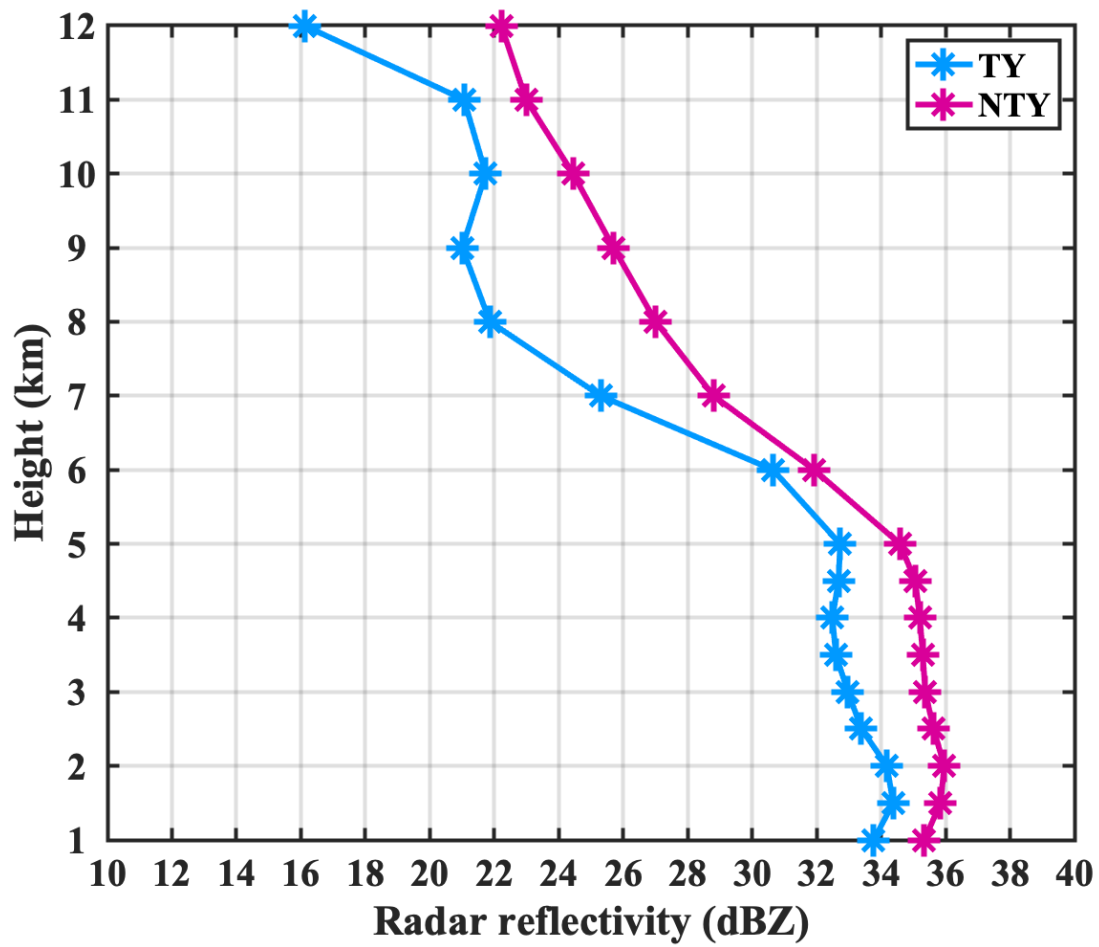


Figure 19. Mean radar reflectivity profiles of typhoon (TY) and non-typhoon (NTY) rainfall.